Precision Mechanics & Digital Fabrication
https://www.acadlore.com/journals/PMDF

3D-Printed Structured Adsorbents for Wastewater Treatment: Balancing Hierarchical Pore Design and Mechanical Robustness

Tanghui Ding, Lu Zhang*

College of Construction Engineering, Jilin University, 130026 Changchun, China

* Correspondence: Lu Zhang (lu_zhang@jlu.edu.cn)

Received: 07-10-2025 **Revised:** 09-12-2025 **Accepted:** 09-23-2025

Citation: T. H. Ding and L. Zhang, "3D-printed structured adsorbents for wastewater treatment: Balancing hierarchical pore design and mechanical robustness," *Precis. Mech. Digit. Fabr.*, vol. 2, no. 4, pp. 189–221, 2025. https://doi.org/10.56578/pmdf020401.

Abstract: 3D printing provides an effective digital fabrication route for manufacturing structured adsorbents with customized geometries, offering clear advantages in permeability, recoverability, and structural integration for water treatment applications. However, a fundamental challenge remains: high porosity, which is essential for mass transfer and adsorption capacity, often compromises mechanical robustness, thereby limiting structural stability, recyclability, and service life under dynamic operating conditions. Most existing studies address this trade-off through incremental optimization within individual material systems, resulting in limited performance improvement. This review systematically summarizes recent advances in 3D-printed structured adsorbents by taking adsorption mechanisms as the central framework. Strategies for enhancing mass transfer through hierarchical pore architecture are reviewed alongside a critical analysis of chemical durability and mechanically governed structural stability, which are key factors for engineering reliability. Emerging fabrication approaches, including core-shell printing and multi-material co-extrusion, are discussed as promising routes to decouple adsorption functionality from load-bearing structures, enabling the concurrent improvement of adsorption performance and mechanical integrity. In addition, challenges related to performance evaluation, dynamic adsorption testing, and cost-benefit considerations are examined, providing guidance for the transition from material-level printing toward structurally reliable adsorption device design.

Keywords: 3D printing; Structured adsorbents; Hierarchical pores; Mechanical robustness; Wastewater treatment

1 Introduction

The global challenge of water pollution has intensified in recent decades, exerting profound and long-lasting impacts on ecological systems, public health, and socioeconomic development [1]. Rapid industrialization, urban expansion, and agricultural intensification have resulted in the continuous discharge of domestic sewage, agricultural runoff, and industrial effluents into natural water bodies, accelerating the degradation of freshwater ecosystems. In many regions, the effectiveness of water pollution control is further constrained by insufficient monitoring data, fragmented management systems, and a severe shortage of financial resources dedicated to treatment infrastructure and technological upgrades [2]. In addition to conventional pollutants such as nutrients and heavy metals, water environments are increasingly burdened by a diverse range of emerging organic pollutants, characterized by high persistence, strong concealment, and complex chemical structures that complicate detection and remediation [3–5]. As a result, heavy metals, dyes, and emerging contaminants continue to demand sustained attention due to their toxicity, bioaccumulation potential, and resistance to conventional treatment processes.

To mitigate these challenges, a variety of water treatment technologies have been developed and applied, including coagulation [6], catalytic oxidation [7], membrane separation [8], biological treatment [9], and adsorption [10]. Among these approaches, adsorption has attracted enduring interest owing to its operational simplicity, high removal efficiency, adaptability to diverse pollutants, and suitability for both centralized and decentralized treatment scenarios [11]. Adsorption processes rely on porous solid materials to capture contaminants through surface interactions, making the physicochemical properties and structural configuration of adsorbents decisive factors in treatment performance. Nevertheless, conventional adsorbents frequently suffer from intrinsic limitations, such as poor selectivity, particle agglomeration in powdered forms, difficulties in post-treatment recovery, risks of secondary

pollution, insufficient permeability in bulk configurations, low utilization efficiency of active sites, and limited regenerability.

In response to these limitations, current research efforts have increasingly focused on the construction of 3D structured adsorbents, the development of novel adsorption materials, and the modification of traditional adsorbent systems. Within this context, 3D printing—also referred to as additive manufacturing—has emerged as a disruptive digital fabrication technology with the capability to reshape the design and manufacturing paradigm of functional adsorption devices. Since its introduction in the late twentieth century, 3D printing has been widely adopted across multiple industrial sectors due to its inherent advantages in geometric freedom, design flexibility, rapid prototyping, and on-demand customization [12, 13]. By enabling layer-by-layer fabrication guided by computer-aided design, 3D printing facilitates the precise control of macroscopic geometry and internal architecture, offering a viable route to overcome the manufacturing constraints associated with conventional techniques such as templating, foaming, casting, and self-assembly.

From a manufacturing perspective, 3D printing provides unique opportunities to integrate adsorption functionality with structural design, thereby addressing long-standing challenges related to mass transfer efficiency, hydraulic permeability, and mechanical stability. Certain printing techniques allow the incorporation of advanced adsorption materials without altering their intrinsic properties, while most additive manufacturing processes are compatible with subsequent chemical modification or surface functionalization. Consequently, 3D printing has been increasingly recognized as an enabling platform for the fabrication of structured adsorbents tailored for water treatment applications. Although the application of 3D printing in this field remains at an early stage, publication trends indicate rapid growth and expanding research interest (as shown in Figure 1).

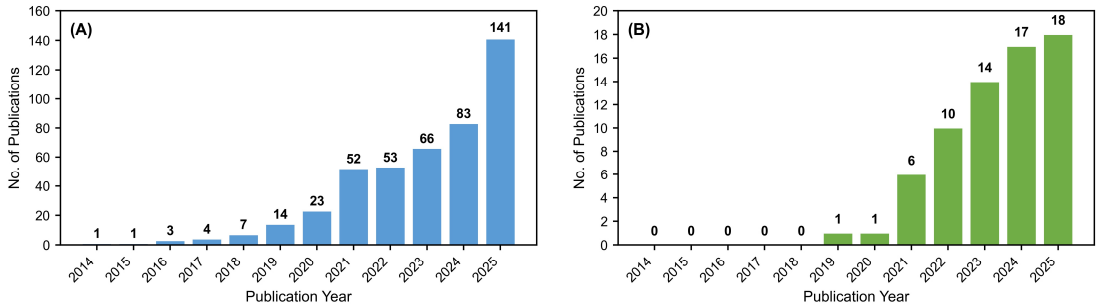

Figure 1. Publication trends in 2014–2025: (a) wastewater 3D printing; (b) wastewater 3D printing adsorbent

Previous review studies have examined the use of 3D printing in water pollution control from broad perspectives, encompassing 3D-printed membranes and membrane supports, catalytic reactors, biological carriers, and structured adsorbents, including fixed-bed adsorption systems [14–16]. Other reviews have focused on specific material classes and their integration with 3D printing, reporting advances across multiple application domains [17–19]. However, existing reviews generally provide limited and fragmented coverage of 3D-printed adsorption systems. Most emphasize maximum adsorption capacity as the primary performance indicator, while offering insufficient analysis of hierarchical pore architecture design, chemically and mechanically governed stability, and dynamic adsorption behavior—factors that are critical for long-term operation and engineering feasibility.

Against this background, the present review aims to systematically summarize recent progress in the fabrication of structured adsorbents for water treatment using diverse 3D printing technologies, with adsorption mechanisms serving as the central organizing framework. Emphasis is placed on elucidating how synergistic macro–micro structural design influences mass transfer pathways and adsorption kinetics, as well as on critically examining the chemical durability and mechanical robustness that dictate recyclability and service reliability. Furthermore, key challenges such as ambiguous performance comparison standards, inadequate evaluation of dynamic adsorption processes, and the lack of comprehensive cost-benefit analysis are discussed. By bridging concepts from precision manufacturing, structural mechanics, and functional materials engineering, this review seeks to provide guidance for advancing 3D-printed adsorbents from exploratory material printing toward mechanically reliable, application-oriented, and digitally manufactured adsorption devices.

2 Digital Fabrication Technologies for Manufacturing Structured Adsorbents

According to the classification system established by the ISO, additive manufacturing technologies can be categorized into seven principal types: powder bed fusion [20], binder jetting [21], directed energy deposition [22], material jetting [23], material extrusion [24], sheet lamination [25], and vat photopolymerization [26]. Each category is characterized by distinct material feedstocks, energy delivery mechanisms, and consolidation principles, which

collectively determine the achievable geometric precision, internal architecture, and mechanical integrity of printed components.

Among these technologies, material extrusion and vat photopolymerization have emerged as the most mature and widely adopted approaches for the fabrication of 3D structured adsorbents. Their dominance arises from a favorable balance between material compatibility, process controllability, and structural design freedom. In addition, selective laser sintering (SLS), a representative powder bed fusion technique, has recently attracted preliminary attention due to its ability to fabricate self-supporting porous structures with inherently high mechanical strength. Although the application scope of SLS in adsorbent preparation remains limited at present, its potential for producing mechanically robust adsorption frameworks warrants further exploration. Collectively, these technologies provide complementary manufacturing routes for constructing structured adsorbents with tailored pore architectures and functional performance, making them particularly relevant to precision manufacturing-oriented adsorption device design.

2.1 Material Extrusion Technology

Material extrusion technologies, primarily including fused deposition modeling (FDM) and direct ink writing (DIW), fabricate 3D objects through the continuous extrusion of thermally softened materials or viscoelastic slurries, followed by layer-by-layer deposition and solidification. Owing to their operational simplicity, scalability, and broad material adaptability, material extrusion techniques currently represent the most extensively explored category for the preparation of 3D-printed adsorbents.

FDM operates by heating thermoplastic polymers to a semi-molten state and extruding them through a nozzle to construct predefined geometries via successive layer stacking. Due to its low equipment cost, high process stability, and ease of implementation, FDM is among the most mature and widely utilized additive manufacturing techniques [27]. However, the thermoplastic materials commonly employed in FDM, such as polylactic acid (PLA), acrylonitrile–butadiene–styrene, and polyamide (PA) [28], generally exhibit negligible intrinsic adsorption capacity. As a result, the fabrication of functional adsorbents using FDM typically relies on two main strategies. The first strategy involves post-processing modification of the printed thermoplastic scaffold to introduce adsorption-active sites through chemical functionalization or surface coating [29]. The second strategy focuses on the preparation of composite filaments by incorporating adsorptive fillers into thermoplastic matrices prior to printing, thereby integrating structural formability with adsorption functionality [30, 31].

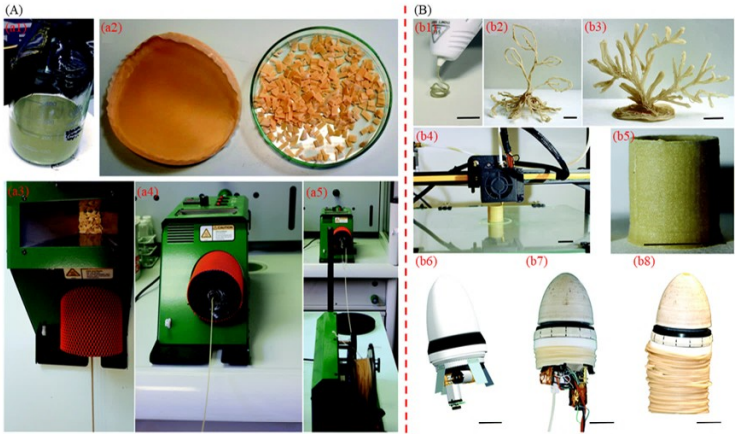

Figure 2. Schematic illustration of a material extrusion-based fabrication route for structured adsorbents using polycaprolactone (PCL)/sodium alginate (SA) composite filaments
Reprinted with permission from Ref. [31] © 2020 Royal Society of Chemistry

Note: (A) Fabrication process of PCL/SA composite filaments: (a1) Blended dichloromethane (DCM) solution of SA and PCL; (a2) Composite film formed after DCM volatilization and its cut fragments; (a3–a5) Preparation of PCL/SA filaments via heating and extrusion of composite fragments using a hot extruder. (B) 3D printing of adsorption devices using PCL/SA composite filaments: (b1–b3) 3D printing pen and the plant-like, algae-like adsorbents printed by it; (b4–b5) Operating fused deposition modeling (FDM) 3D printer and the tubular adsorbents printed by it; (b6–b8) Specially designed growth robot model, physical prototype, and the root-like structures printed by it

Figure 2A schematically illustrates a representative process for fabricating composite filaments using sodium alginate (SA) as an adsorptive component and polycaprolactone (PCL) as a thermoplastic matrix. In this approach, SA is dissolved at a predetermined ratio in a dichloromethane (DCM) solution containing PCL (a1). After solvent evaporation, the resulting composite film is cut into fragments (a2), which are subsequently fed into a hot extruder for melting and extrusion to produce PCL/SA composite filaments with combined adsorptive and thermoplastic

characteristics (a3–a5). These filaments can then be employed for the fabrication of structured adsorbents using various printing modalities, as shown in Figure 2B. Free-form adsorbents can be manually fabricated using a 3D printing pen (b1–b3), while geometrically defined structures, such as cylindrical adsorbents, can be produced using conventional FDM printers (b4–b5). Moreover, bioinspired architectures, including root-mimetic structures, can be realized through specialized growth-based robotic printing systems (b6–b8). Such examples highlight the versatility of FDM in generating complex macroscopic geometries, albeit with limitations in fine structural resolution and interlayer bonding strength.

DIW differs fundamentally from FDM in that it employs viscoelastic inks composed of solid powders dispersed in liquid media, which are extruded through a nozzle under applied pressure to form self-supporting structures [32]. DIW exhibits exceptional material compatibility, encompassing inorganic ceramics, carbon-based materials, polymer hydrogels, and composite systems, thereby offering a highly flexible platform for fabricating customized functional adsorbents [33]. The success of DIW critically depends on ink formulation, which must satisfy stringent rheological requirements, including pronounced shear-thinning behavior to ensure smooth extrusion, as well as sufficient yield stress and elastic recovery to maintain structural fidelity after deposition. In current practice, DIW-based adsorbent fabrication typically involves dispersing adsorptive powders, such as metal–organic frameworks (MOFs) or biochar, into liquid binders, followed by printing and subsequent post-processing steps, including drying, crosslinking, or sintering, to generate porous adsorption architectures [34]. Compared with FDM, DIW offers superior control over internal pore networks and material distribution, but often at the expense of reduced mechanical robustness and increased sensitivity to processing conditions.

2.2 Vat Photopolymerization Technology

Vat photopolymerization technologies, represented by stereolithography apparatus (SLA) and digital light processing (DLP), fabricate 3D structures through the selective curing of liquid photosensitive resins using ultraviolet light.

In SLA, a focused laser beam scans the resin surface along predefined paths to solidify each layer, whereas DLP employs a projected light pattern to cure an entire layer simultaneously, resulting in higher fabrication efficiency. Both techniques are capable of producing complex geometries with exceptionally high dimensional accuracy, surface quality, and feature resolution [35, 36], making them particularly attractive for precision manufacturing applications.

In addition to conventional SLA and DLP, advanced vat photopolymerization approaches employing full-surface curing but alternative projection mechanisms have been developed, including Masked Stereolithography (MSLA), also known as liquid crystal display (LCD)-based stereolithography, and Mask-Image-Projection-based Stereolithography (MIP-SL) [37, 38]. Despite their technical advantages, the application of vat photopolymerization in adsorbent preparation remains relatively limited, primarily due to the chemical sensitivity and functional constraints of commercially available photosensitive resins. The restricted material palette poses challenges for directly imparting adsorption functionality, thereby limiting large-scale adoption.

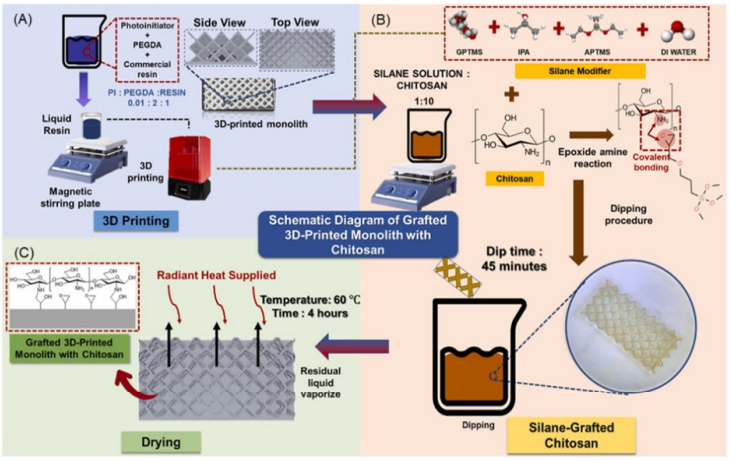

Figure 3. Schematic illustration of a vat photopolymerization-based fabrication route for structured adsorbents: (A) fabrication of PEG200DA-based 3D-printed template; (B) surface modification of the 3D-printed template; and (C) acquisition of the final 3D structured adsorbent via post-treatment
Reprinted with permission from Ref. [41] © 2022 Elsevier

Current research efforts generally follow two main pathways. The first involves incorporating micro- or nano-scale adsorptive particles into photosensitive resins to form composite systems that retain photocurability while introducing adsorption capacity [39]. The second pathway focuses on fabricating high-precision structural skeletons via vat photopolymerization, followed by post-printing surface functionalization to impart adsorption activity [40, 41]. As illustrated in Figure 3, a composite ink composed of glycol diacrylate (PEG200DA), photocurable resin, and a photoinitiator is used to fabricate a structured template via DLP printing (A). The printed scaffold is subsequently immersed in a coupling agent solution containing glycidyloxypropyl trimethoxysilane and (3-aminopropyl) trimethoxysilane (APTMS) to achieve surface modification (B). After rinsing and drying, a 3D structured adsorbent with tailored surface functionality is obtained (C). This strategy underscores the strength of vat photopolymerization in delivering geometrically precise frameworks, while highlighting the reliance on secondary modification to achieve functional performance.

2.3 Powder Bed Fusion Technology

SLS is a representative powder bed fusion technology that employs a high-energy laser beam to selectively sinter polymer or metal powders in a layer-by-layer manner, forming 3D structures without the need for additional binders [42]. This process enables the direct fabrication of porous components with high mechanical strength, thermal stability, and structural integrity—properties that are difficult to achieve with extrusion- or photopolymerization-based methods. From a manufacturing perspective, SLS has clear advantages in fabricating mechanically robust adsorption frameworks or load-bearing skeletons that can be functionalized for adsorption. Its inherent strength and interconnected porosity make it well-suited for dynamic flow and long-term service. However, SLS's application in adsorbent preparation is still at an early stage, mainly limited by the lack of powders with intrinsic adsorption properties, as well as high process costs and energy consumption. Further research is needed to expand material options and integrate SLS with post-processing or hybrid manufacturing for advanced adsorption devices.

3 Material Systems and Manufacturing Characteristics of 3D-Printed Adsorbents

Adsorption interactions encompass a wide range of physicochemical mechanisms, including electrostatic interactions (van der Waals forces), chemical bonding interactions (covalent bonds, ionic bonds, and coordination bonds), electrostatic attraction processes (ion exchange and Coulombic attraction), hydrophobic interactions driven by entropy effects, π–π conjugation or stacking interactions arising from delocalized π-electron clouds between aromatic structures, hydrogen bonding interactions as specific strong dipole–dipole forces, and biospecific adsorption based on molecular recognition [43–45]. Regardless of the dominant interaction mechanism, adsorption fundamentally occurs at the solid–liquid interface. Consequently, specific surface area and pore architecture—particularly the presence and connectivity of micro- and mesopores-constitute the primary physical parameters governing adsorption capacity and mass transfer behavior. Based on these principles, a wide spectrum of materials, ranging from conventional high-surface-area adsorbents such as activated carbon and zeolites to porous polymers and even various industrial wastes, have been extensively developed and employed as adsorption media [46–49].

When these materials are fabricated into structured adsorbents via 3D printing, however, their design and application paradigm undergoes a substantial transformation from a manufacturing perspective. In contrast to conventional particulate or bulk adsorbents, 3D printing imposes additional and often stringent requirements on material systems, extending beyond adsorption performance to include printability-related properties such as rheological behavior, curing characteristics, shape retention, and interlayer bonding stability. As a result, materials suitable for 3D-printed adsorbents must achieve a delicate balance between microscale adsorption activity and macroscale formability, ensuring that functional performance is preserved while structurally robust architectures can be reliably manufactured.

To address these constraints, extensive efforts have been devoted to the targeted adaptation and modification of diverse material systems. Strategies include tailoring material composition to improve extrusion or curing behavior, introducing binders or secondary phases to enhance structural integrity, and designing composite systems that decouple adsorption functionality from load-bearing frameworks. Representative examples of 3D-printed adsorbents fabricated from different material systems and structural designs are illustrated in Figure 4, highlighting the diversity of achievable architectures, surface morphologies, and internal pore structures.

Figure 4 presents typical 3D printed adsorbents with various materials and geometries (A), their characteristic rough surface features (B), and representative microporous structures revealed by scanning electron microscopy at magnifications of $50\times$ and $2000\times$ (C), respectively. These structural features collectively reflect the interplay between material selection, fabrication strategy, and resulting adsorption functionality.

Table 1, Table 2, Table 3, Table 4, and Table 5 summarize representative studies published from 2014 to the present on the fabrication of adsorbents and fixed-bed adsorption devices for water pollution treatment using 3D printing technologies. Each study summarizes its material system, fabrication method, and key performance.

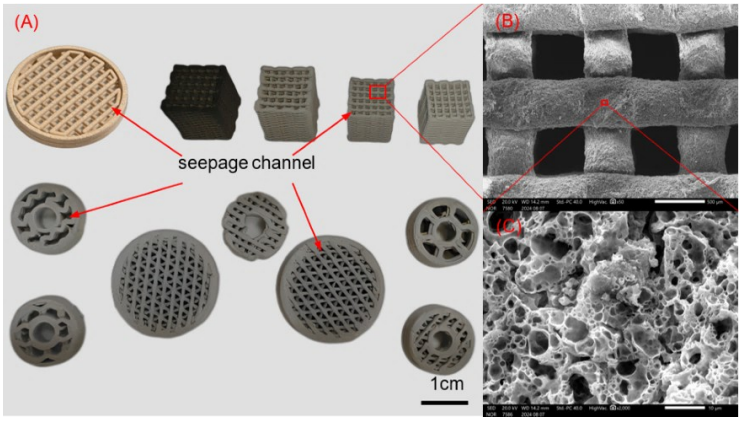

Figure 4. Representative 3D-printed structured adsorbents illustrating material diversity, surface morphology, and hierarchical pore architecture: (A) 3D-printed adsorbents fabricated from different material systems and structural designs; (B) surface morphology of printed adsorbents; and (C) microporous features revealed by scanning electron microscopy (SEM) at magnifications of 50× and 2000×, respectively

The listed adsorption performances are optimal values under specific experimental conditions, so they are not suitable for direct quantitative comparison across studies. Instead, they demonstrate the range of material–process combinations investigated. In the following sections, the major material systems successfully employed in 3D-printed adsorbents are systematically reviewed, with particular emphasis on the strategies adopted to simultaneously achieve adequate printability, structural stability, and high adsorption efficiency.

3.1 Polymer Materials

Common natural polymer materials for adsorption include chitosan (CS) and SA. Chitosan is a natural biopolymer synthesized by deacetylation of chitin. It is an unbranched polysaccharide, commonly found in shrimp shells and crab shells. It is rich in amino and hydroxyl groups and can adsorb heavy metals and dyes through chelation and electrostatic interactions. Appuhamillage et al. [50] successfully prepared a series of cDAP 3D-printed hydrogel adsorbents using diacrylated Pluronic F-127 (DAP) and chitosan (Figure 4A). The optimal formulation cDAP-1X (1 wt% chitosan + 25 wt% DAP) has both good printability and mechanical strength (Young's modulus 1.93 kPa), and can print thin sheets, cups, and complex internal pore structures. It has excellent adsorption effects on four heavy metals: within 30 minutes, the removal rates of Cu^{2+} (1500 ppb), Cd^{2+} (30 ppb), and Hg^{2+} (10 ppb) reach 95%, and the concentrations are reduced below the EPA safety standards; the removal rate of Pb^{2+} (30 ppb) in complex structure B is 74% within 10 minutes, and the efficiency remains 98% after 5 cycles. Husna et al. [41] obtained a 3D PEGDA monolithic skeleton through vat photopolymerization technology. Chitosan is covalently grafted onto the PEGDA skeleton through silane coupling agents, significantly improving mechanical performance (storage modulus 427.73 MPa) and structural stability. Under optimal conditions (chitosan concentration 2 wt%, soaking time 45 minutes, pH = 6.3, 60°C), the maximum adsorption capacity for methyl orange is 12.7 mg/g, and the removal rate is 90.4%. The adsorption process conforms to the Langmuir isotherm model and pseudo-second-order kinetic model. The BOD removal rate for actual textile wastewater reaches 62.4%, while the COD removal rate is relatively low (2%); the adsorbent can be recycled 4 times, and the removal rate remains 78% after 4 cycles, which can be simply regenerated by desorption with deionized water rinsing.

Table 1 summarizes recent research on natural and synthetic polymers for 3D-printed adsorbents in water pollution treatment. Abbreviations for target pollutants are listed below: KZ-Ketoconazole; CZ-Clotrimazole; MZ-Miconazole; Rh B-Rhodamine B; DNBP-Dinitro butylphenol; RO16-Reactive Orange 16; MB-Methylene Blue; MO-Methyl Orange; CR-Congo Red; PVP-I-Povidone-Iodine; IPA-Isopropanol; $MeHg^{+}$-Methylmercury; iHg^{2+}-Inorganic Mercury; MG-Malachite Green.

Table 1. Representative material systems and fabrication characteristics of 3D-printed structured adsorbents for water pollution treatment (2014–present)

Materials	Printing Techniques	Targeted Contaminants	Adsorption Capacity	Adsorption Rate	Ref.
sodium alginate (SA) Cellulose Nanocrystals	direct ink writing (DIW)	Cu^{2+}	68 mmol/g	—	[51]

SA	DIW	U^{6+}	117.3 mg/g (pH = 2.5); 410.1 mg/g (pH = 7.4)	71.5% (pH = 2.5) 98.47% (pH = 7.4)	[52]
Chitosan	DIW	Pb^{2+} Cu^{2+} Cd^{2+} Hg^{2+}	Pb^{2+}: 0.6 mg/g Cu^{2+}: 0.55 mg/g Cd^{2+}: 0.52 mg/g Hg^{2+}: 0.5 mg/g	Pb^{2+}: 95% (10 min) Cu^{2+}: 95% (30 min) Cd^{2+}: 95% (30 min) Hg^{2+}: 95% (30 min)	[50]
SA (Na-alginate) Nano-Clay (Cloisite® 20A)	DIW	Pb^{2+}	532 mg/g (EB15 15 kGy Electron Beam Crosslinking)	98% (Initial Concentration 500 mg/L EB15)	[53]
Starch Gelatin Melamine	DIW	MB	68.9 mg/g	93.2% (NPCR-50) 93.0% (NPCR-350)	[54]
Cyclodextrin Polymer Graphitic Carbon Nitride (g-C_3N_4)	digital light processing (DLP)	MB Rh B MO CR	MB: 4.27 mg/g Rh B > MO > CR	MB: 91% Rh B: 86% MO: 81% CR: 53%	[39]
Chitosan	DLP	MO	12.7 mg/g	90.40%	[41]
Methacrylated Starch ACy	DLP	MB	61.24 mg/g	—	[55]
polycaprolactone (PCL)/sodium alginate (SA)	fused deposition modeling (FDM)	Cu^{2+}	93.3 mg/g (PCL/30% SA 0.17% w/w Cu_2SO_4 30 d)	91.5% (PCL/30% SA 0.17% w/w Cu_2SO_4 30 d)	[31]
polylactic acid (PLA)	FDM	KZ CZ MZ	—	KZ: 39.12%–40.68% CZ: 78.96%–79.95% MZ: 69.62%–70.58%	[29]
Conductive PLA Carbon Black	FDM	Benzene Toluene Ethylbenzene	—	Benzene: 50.6% Toluene: 81.3% Ethylbenzene: 92.0%	[56]
LAY-FOMM®60 Filament (Blend Polymer of Polyvinyl Alcohol and Polyurethane)	FDM	Fe^{2+} Cu^{2+} Zn^{2+}	—	Fe^{3+}: >80% Cu^{2+}: >80% Zn^{2+}: >80%	[57]
Polyvinyl Alcohol Acrylic Acid	FDM	Pb^{2+} DNBP	Pb^{2+}: 896 mg/g	Pb^{2+}: 100% DNBP: COD Removal Rate 73%	[58]
Chitosan Hydroxyapatite	FDM	Cu^{2+}	119 ± 1 mg/g (298 K Fitted by Langmuir Model)	Static Adsorption: ≥ 98% Dynamic Adsorption: 99.95% (10 mL/min 10 h)	[30]
Thermoplastic Polyurethane Elastomer	FDM	Trypan Blue PVP-I IPA Olive Oil Mineral Oil	—	Trypan Blue: >90% PVP-I: >90% IPA: >90% Olive Oil: 60% Olive Oil: 27%	[59]
Calcium-Based MOFs (Ca-MOF) Calcium Silicate ($CaSiO_3$)	FDM	MB	2.35 mg/g (50 mg/L) 4.6 mg/g (100 mg/L) 8.18 mg/g (200 mg/L)	88% (50 mg/L and 100 mg/L)	[60]

Poly (ethylene glycol) Diacrylate Hydroxyethyl Methacrylate	Masked Stereolithography (MSLA)	Rh B	3.73 mg/g (Initial Concentration 100 ppm 50℃ 1 Lattice)	94.86% (Initial Concentration 20 ppm 50℃ Dosage 3 Lattices)	[61]
Polyamidoxime	MSLA	U^{6+}	78.01 mg/g (Fitted by Langmuir Isotherm Model 25℃ pH = 6.0)	—	[62]
Chitosan GO	MSLA	MO	182.33 mg/g	91.16%	[63]
Nano-Chitosan	MSLA	MO	12.2 ± 0.7 mg/g	96% (80 min)	[64]
Chitosan	stereolithography apparatus (SLA)	Cu^{2+}	13.7 mg/g	92%	[65]
Thiol Monomer (Pentaerythritol Tetra (3-mercaptopropionate) PETMP) Alkyne Monomer (3-Butyn-1-ol BA)	SLA	Malachite Green (MG)	588 ± 16 mg/g	—	[66]
Thiol-Functionalized Silica Gel (SiliaMetS Thiol)	selective laser sintering (SLS)	$MeHg^{+}$ iHg^{2+}	iHg^{2+}: 220 mg/g	$MeHg^{+}$: 96.1% iHg^{2+}: 100%	[67]
PA-12	SLS	17β-Estradiol	71 ± 6 μg/g	100% (Dynamic Adsorption)	[68]

Note: CR—Congo Red; MB—Methylene Blue; Rh B—Rhodamine B; MG—Malachite Green; CV—Crystal Violet; MV—Methyl Violet; AO—Auramine O; MO—Methyl Orange; DR31—Direct Red 31; 2-CP—2-Chlorophenol; 4-CP—4-Chlorophenol; 2,4-DCP—2,4-Dichlorophenol; 2,4,6-TCP—2,4,6-Trichlorophenol; PCP—Pentachlorophenol; 4-NP—4-Nitrophenol; BPA—Bisphenol A; EB—Evans Blue

SA is a by-product after extracting iodine and mannitol from brown algae such as kelp or giant kelp. It is also a natural polysaccharide rich in carboxyl groups. It can adsorb cations through ion exchange and is often used as a gel carrier. Fuxiang et al. [52] prepared 3D SA adsorbents through DIW 3D printing combined with calcium ion crosslinking technology. Its hierarchical porous structure (average pore size about 500 μm) provides abundant adsorption sites and rapid mass transfer channels, with low volume shrinkage rate and strong structural stability. The adsorption mechanism of the adsorbent is the synergistic effect of electrostatic interaction and ion exchange: the oxygen-containing functional groups on the surface of SA have electrostatic attraction with U^{6+}, and at the same time, Ca^{2+} undergoes ion exchange with U^{6+}, and there is no redox reaction during the adsorption process (U always exists in the hexavalent form). The 3D SA adsorbent has a wide applicable pH range (3–10), and performs particularly well under acidic conditions (adsorption capacity 117.3 mg/g at $pH = 2.5$). After soaking in 3.6×10^{-3}–2.0 mol/L HCl solution for 24 hours, the structure does not collapse and the adsorption performance does not decrease significantly.

Liakos et al. [31] successfully prepared PCL/SA composite thermoplastic filaments by fusing PCL and SA. PCL and SA form hydrogen bonds through hydroxyl and carbonyl groups, making the filaments have good stability in deionized water (no SA leakage when SA content $\leq$ 15%), and the stability is further improved in solutions containing copper ions (Cu^{2+} can crosslink SA). The copper ion adsorption capacity of the composite filaments is positively correlated with the SA content. The maximum adsorption capacity of PCL/30% SA filaments reaches 93.3 mg/g (0.17% w/w Cu_2SO_4 solution, 30 days). The adsorption mechanism is mainly ion exchange between Na^{+} in SA and Cu^{2+}, and at the same time, Cu^{2+} forms bidentate coordination bonds with the carboxyl groups of SA.

Organic polymers also belong to polymer materials. Among them, common 3D printing materials such as PLA, photosensitive resins, and polyethylene glycol diacrylate are often used as skeleton support materials for adsorbents and have almost no adsorption performance themselves. In addition, researchers have newly discovered some polymers with adsorption effects.

Polypyrrole is a conductive polymer material formed by polymerization of pyrrole monomers. The functional groups in its structure can directly adsorb pollutants through electrostatic, hydrogen bond and other interactions.

This material is generally used to encapsulate composite adsorbent precursors to fix high-performance adsorption materials and provide additional adsorption sites [40, 69].

Cyclodextrin polymers are a series of cyclic oligosaccharides generated from amylose under the action of cyclodextrin glucosyltransferase produced by Bacillus. Their outer surface is rich in hydroxyl groups and is generally hydrophilic; the interior forms a relatively hydrophobic cavity that can accommodate hydrophobic guest molecules and can specifically adsorb small organic molecules through "host-guest" inclusion interactions. Noè et al. [55] used linear corn starch to prepare methacrylated starch (MS), dissolved γ-cyclodextrin in anhydrous N-methyl pyrrolidone, and added acryloyl chloride dropwise at 0℃ to prepare acrylated γ-cyclodextrin (ACy). After mixing in different proportions, adsorbents with complex 3D structures and good mechanical stability (compression modulus 0.36–3.93 MPa) were obtained through DLP technology. Adsorption comparison experiments showed that the maximum adsorption capacity of MS-ACy composite adsorbents for methylene blue reaches 61.24 mg/g, and the adsorption kinetics conforms to the pseudo-second-order model (R^2 >0.996), indicating that chemical adsorption is dominant; the introduction of ACy improves the adsorption capacity through host-guest inclusion interactions, and the adsorption effect is optimal when the mass ratio of MS to ACy is 1:1 to 1:2 (Figure 5 C).

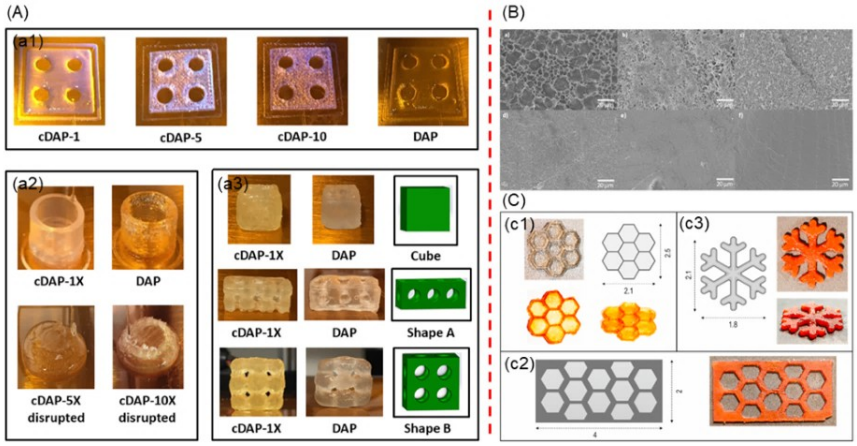

Figure 5. Polymer-based 3D printing adsorbents
Reprinted with permission from Ref. [50] © 2019 Society of Chemical Industry
Reprinted with permission from Ref. [55] © 2021 Elsevier

Note: (A) cDAP hydrogel-based adsorbents with different material ratios and structures: (a1) sheet-shaped, (a2) cup-shaped (printability decreases as the chitosan content increases), (a3) cube-shaped; (B) Field emission scanning electron microscopy (FESEM) images of hydrogels with different material ratios; from left to right and top to bottom, the content of methacrylate starch (MS) decreases gradually while the content of ACy increases gradually; and (C) MS-ACy hydrogel adsorbents printed via DLP technology: (c1) MS-ACy 1:1, (c2–c3) MS-ACy 1:2

3.2 Advanced Functional Materials

MOFs are a class of crystalline porous materials with periodic network structures formed by self-assembly and connection of inorganic metal centers (metal ions or metal clusters) and bridging organic ligands. They have ultra-high specific surface area and adjustable pores, and are high-performance adsorption/catalytic materials. Pei et al. [70] prepared copper-based MOFs Cu-BTC through the reaction of copper nitrate and trimesic acid, dissolved it with SA and gelatin in deionized water to obtain uniform printing ink (Figure 6A. Three structural models (square/hexagon/circle) were designed by CAD, 3D printed by DIW (Figure 6B–E), crosslinked by immersion in $CaCl_2$ solution, and freeze-dried to obtain 3D-printed MOF/CA-GE composite adsorbents. Adsorption experiments showed that the hexagonal printed structure has the optimal adsorption performance, with a MB removal rate of 99.8%, and good adsorption effects on various cationic dyes. The adsorption rate is negatively correlated with the steric hindrance of dyes; moreover, the adsorbent adsorbs rapidly and can reach equilibrium within 20 minutes. In addition, the adsorbent has excellent regeneration performance. It can be recycled 10 times after desorption with 0.1 M hydrochloric acid, and the removal rate is still over 64% in the 10th cycle, which is much better than powdered MOFs.

Table 2 summarizes the latest research progress on advanced functional materials applied in 3D-printed adsorbents for water pollution treatment. Abbreviations of target pollutants are explained as follows: CR—Congo Red; MB—Methylene Blue; Rh B—Rhodamine B; MG—Malachite Green; CV—Crystal Violet; MV—Methyl Violet; AO—Auramine O; MO—Methyl Orange; DR31—Direct Red 31; 2-CP—2-Chlorophenol; 4-CP—4-Chlorophenol; 2,4-DCP—2,4-Dichlorophenol; 2,4,6-TCP—2,4,6-Trichlorophenol; PCP—Pentachlorophenol; 4-NP—4-Nitrophenol; BPA—Bisphenol A; EB—Evans Blue.

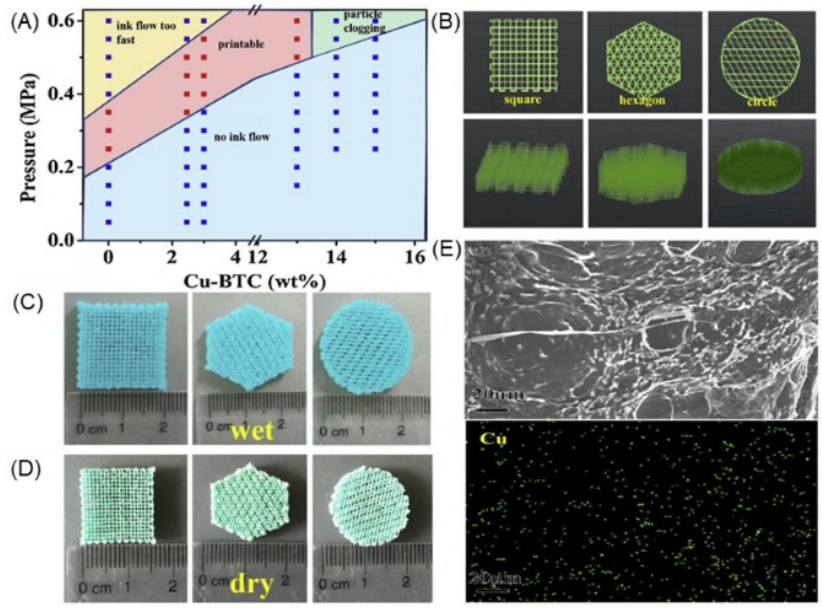

Figure 6. The characterizations of 3D-printed Cu-BTC/CA-GE with different patterns
Reprinted with permission from Ref. [70] © 2020 Elsevier

Note: (A) Printability of Cu-BTC/SA-GE mixed inks; (B) Top view and front view of the three printed computer-aided design (CAD) models; (C and D) The photographs of three print patterns in a wet and dry state, respectively; (E) SEM image and the corresponding EDS elemental mapping of the printed composite (The Cu distribution reveals the dispersion state of Cu-BTC within the calcium alginate and gelatin system)

Table 2. Representative advanced functional material systems and fabrication characteristics of 3D-printed structured adsorbents for water pollution treatment

Materials	Printing Techniques	Targeted Contaminants	Adsorption Capacity	Adsorption Rate	Ref.
Geopolymer, Graphitic Carbon Nitride (g-C_3N_4), GO	DIW	MB	—	93.28% (Photocatalysis + Adsorption); 72.27% (Adsorption Alone)	[71]
Mercapto-GO, Chitosan, ε-Polylysine	DIW	Cu^{2+}	313 mg/g (SGCS-E3, 303.15 K, pH = 5, Initial Concentration 20 mg/L)	—	[72]
Hierarchically Porous Ceramics (3DP-HPC), MOFs	DIW	MB, Rh B, MG, CV	—	MB: 98.34% (3DP-HPC@MIL-100(Fe)); Rh B: 96.93% (3DP-HPC@MIL-100(Fe)); MG: 98.24% (3DP-HPC@HKUST-1); MG: 98.99% (3DP-HPC@MIL-100(Fe)); CV: 97.43% (3DP-HPC@HKUST-1); CV: 98.51% (3DP-HPC@HKUST-1)	[73]

MOFs (Cu-BTC), SA, Gelatin	DIW	MB, MV, MG, Rh B, AO	—	MB: 99.8%; MV: 98%; MG: 83%; Rh B: 79%; AO: 38%	[70]
GO, Chitosan	DIW	Cu^{2+}	269 mg/g (Fitted by Langmuir Model, R^2 = 0.9925, 303.15 K, pH = 5)	84.25% (Dosage 2 g/L, Initial Concentration 20 mg/L, 303.15 K, pH = 5)	[74]
GO, Silicon Carbide (SiC), Geopolymer	DIW	MB	—	88.2% (First Use); 82.0% (After 5 Cycles)	[75]
GO, Polydopamine, Bovine Serum Albumin (BSA)	DIW	Cr^{6+}, Pb^{2+}, MB, EB, n-Hexane, n-Heptane, Toluene	Cr^{6+}: 45.05 mg/g; Pb^{2+}: 43.76 mg/g; MB: 35.33 mg/g; EB: 38.73 mg/g; n-Hexane: Complete Removal; n-Heptane: Complete Removal; Toluene: Complete Removal	Cr^{6+}: 93%; Pb^{2+}: 94%; MB: 99.17%; EB: 87.30%; n-Hexane: 100%; n-Heptane: 100%; Toluene: 100%	[76]
SA, GO	DIW	U^{6+}	740.74 mg/g (3D CG6, Ca^{2+} Single Crosslinking); 847.5 mg/g (3D CG6, Ca^{2+}/Zn^{2+} Double Crosslinking)	99.95% (In the Presence of Competitive Ions)	[77]
MXene ($Ti_3C_2T_x$), MOFs (UiO-66), Polypyrrole	DLP	Cr^{6+}, CR	Cr^{6+}: 40.84 mg/g; CR: 230.96 mg/g	Cr^{6+}: 67.84%; CR: 97.65%	[69]
MXene ($Ti_3C_2T_x$), MOFs (ZIF-67 and MIL-88A (Fe)), Polypyrrole	DLP	CR, Ag^{+}	CR: 1515.15 mg/g; Ag^{+}: 865.35 mg/g	CR: 84.64%; Ag^{+}: 98.56%	[40]
MOFs (Cr-MOF), Nano-Clay (Cloisite® 30B)	DLP	MO, DR31	MO: 1.35 mg/g; DR31: 1.68 mg/g	MO: 74% (pH = 4, 60 min); DR31: 65% (pH = 4, 60 min)	[78]
Graphitic Carbon Nitride (g-C_3N_4)	DLP	Rh B	—	93.46% (Adsorption + Catalysis)	[79]
MXene ($Ti_3C_2T_x$), MOFs (ZIF-8), Chitosan	DLP	MO, DR31	MO: 1.38 mg/g; DR31: 1.27 mg/g	MO: 84.9%; DR31: 91.98%	[80]
Silver-Functionalized Zirconium-Based MOFs (UiO-66-SO_3H@Ag)	DLP	Iodine-131 (^{131}I)	1311 Bq/g	100% (Low Activity 50 Bq Solution); 86% (High Activity 10000 Bq Solution); 90±5% (Hospital Wastewater Recovery)	[81]
Zinc Oxide (ZnO), Titanium Dioxide (TiO_2), Iron-Based MOFs (Fe-MOF)	FDM	Rh B, Ciprofloxacin	—	Rh B: 94.3% (Adsorption + Catalysis); Ciprofloxacin: 42% (Adsorption + Catalysis)	[82]

Two-Dimensional Gadolinium Telluride (Gd_2Te_5)	FDM	MB, MO, Bleaching Powder, Sodium Chloride	—	MB: 69%; MO: 45%; Bleaching Powder: 20%; Sodium Chloride (3.5% NaCl): ¡5%	[83]
Copper-Based MOFs (Cu-MOFs)	FDM	MG	—	$\geq 90\%$	[84]
GO, Chitosan	FDM	CV	46.2 mg/g	$97.8 \pm 0.5\%$ (PLA90%@GO/CS Bionic Filter)	[85]
Copper-Based MOFs (Cu-BTC)	FDM	MB	64.3 mg/g (10 mg/L Solution)	93.3% (10 mg/L Solution)	[86]
Iron-Based MOFs (MIL-100 (Fe))	SLA	2-CP, 4-CP, 2,4-DCP, 2,4,6-TCP, PCP, 4-NP, BPA	—	2-CP: 93%-109%; 4-CP: 93%-109%; 2,4-DCP: 93%-109%; 2,4,6-TCP: 93%-109%; PCP: 93%-109%; 4-NP: 93%-109%; BPA: 93%-109% (Spiked Recovery Rate)	[87]
MOFs (ZIF-67, NH_2-MIL-101 (Al), MOF-801, HKUST-1, ZIF-8)	SLS	MB	222 mg/g (NH_2-MIL-101 (Al))	81.3% (NH_2-MIL-101 (Al), After 5 Cycles)	[88]

Note: CR—Congo Red; MB—Methylene Blue; Rh B—Rhodamine B; MG—Malachite Green; CV—Crystal Violet; MV—Methyl Violet; AO—Auramine O; MO—Methyl Orange; DR31—Direct Red 31; 2-CP—2-Chlorophenol; 4-CP—4-Chlorophenol; 2,4-DCP—2,4-Dichlorophenol; 2,4,6-TCP—2,4,6-Trichlorophenol; PCP—Pentachlorophenol; 4-NP—4-Nitrophenol; BPA—Bisphenol A; EB—Evans Blue

Graphene oxide (GO) is a graphene derivative. Graphene itself is an allotrope of carbon, and carbon atoms are bonded with sp^2 hybridization to form a single-layer hexagonal honeycomb lattice graphene. Using strong oxidants to react with graphite or graphene can insert a large number of oxygen-containing groups between graphite layers and expand the interlayer spacing, facilitating the entry of substances. It has a huge specific surface area and rich oxygen-containing functional groups, and can adsorb pollutants through various interactions. Zhang et al. [74] successfully prepared 5 types of GO/CS composite adsorbents with different proportions through DIW 3D printing. Among them, the optimal formulation G8/C7 (8 wt% GO + 7 wt% CS) has both high adsorption activity and mechanical strength, and excellent acid-base resistance. It can maintain structural integrity for 180 days under pH 3–9 conditions. In addition, the maximum adsorption capacity of G8/C7 for Cu^{2+} is 269 mg/g (Langmuir model). The adsorption mechanism includes electrostatic interaction, van der Waals force, and coordination chelation of nitrogen-containing/oxygen-containing functional groups, belonging to monolayer chemical adsorption. In cyclic adsorption experiments, the adsorption capacity retains 71% after 6 cycles, and the mechanical strength reaches 5.85 MPa, which is both practical and economical, and very suitable for copper-containing wastewater treatment. Yong et al. [63] successfully prepared a SiOC ceramic matrix through LCD 3D printing and pyrolysis technology, and grafted a chitosan-GO composite layer mediated by GLYMO to form a high-strength and high-stability adsorbent. The BET specific surface area reaches 78.90 m^2/g (much higher than 1.21 m^2/g of pure SiOC). Under optimal conditions (GO/C = 0.1, 30°C, pH = 3.0), the adsorption capacity of the adsorbent for MO is 182.33 mg/g, and the adsorption rate is 91.16%. The adsorption mechanism includes electrostatic interaction between -NH_3^+ of chitosan and MO-SO_3^-, and π-π stacking interaction between GO and MO. The adsorption process conforms to the Harkins-Jura isotherm model and pseudo-second-order kinetic model, and the adsorption spontaneity is the strongest at 30°C; the removal rate is still over 92% after 5 cycles, and the desorption and regeneration effects are stable. The SiOC ceramic matrix endows the adsorbent with excellent mechanical strength (elastic modulus 185.9 kPa) and thermal stability, solving the pain points of traditional adsorbents being easy to break and difficult to recover.

The precursor of the emerging material MXene is the ternary layered MAX phase with the chemical formula $M_{n+1}AX_n$ (M is a transition metal, A is a main group element such as aluminum, and X is carbon or nitrogen).

Graphene-like 2D MXene is obtained by chemically etching the A atomic layer.

Its surface has rich functional groups and strong adsorption performance for heavy metals, dyes, etc. Wu et al. [69] first prepared two-dimensional MXene material TiVCTx and UiO-66, and successfully synthesized TiVCTx/UiO-66 composite material through in-situ growth. Combined with DLP 3D printing and in-situ oxidative polymerization technology, an integral adsorbent PPy/TiVCTx/UiO-66/3DS was prepared, which does not require complex separation and recovery steps and avoids secondary pollution. The adsorbent has excellent adsorption performance for Congo Red (CR) and Cr^{6+}, with maximum adsorption capacities of 230.96 mg/g and 40.84 mg/g, respectively. The adsorption process conforms to the pseudo-second-order kinetic model (dominated by chemical adsorption). The adsorption of CR follows the Freundlich model (multilayer adsorption), and the adsorption of Cr^{6+} follows the Langmuir model (monolayer adsorption). In composite system wastewater, low concentration of Cr^{6+} ($\leq$20 ppm) can promote CR adsorption, while the coexistence of CR will inhibit Cr^{6+} adsorption. The adsorption mechanisms include electrostatic interaction, complexation reaction, redox (reduction of Cr^{6+} to Cr^{3+}), π-π stacking, and pore filling. In addition, the adsorbent has good reusability, maintains a high removal rate after 5 cycles, and has stable fixed-bed dynamic adsorption effect, showing potential for practical wastewater treatment applications.

3.3 Natural Minerals

Clay materials mainly include montmorillonite (MMT), kaolinite, metakaolin, illite, halloysite nanotubes (HNTs), etc. They are all aluminosilicate minerals with high specific surface area and high cation exchange capacity. Due to structural differences, the adsorption capacities of various clay minerals also vary.

Miao et al. [89] successfully prepared MMTNs/GEL/SA composite hydrogel adsorbents through material extrusion 3D printing using montmorillonite nanosheets (MMTNs), gelatin (GEL), and SA. MMTNs are combined with GEL through hydrogen bonds and electrostatic interactions, and then crosslinked with SA to form a stable interpenetrating polymer network (IPN). The material has abundant macropores and sheet structures, which are conducive to the diffusion and adsorption of Pb^{2+}. Under optimal conditions, the maximum adsorption capacity for Pb^{2+} reaches 134 mg/g. The adsorption process is chemical adsorption, and the mechanisms include ion exchange (exchange between Na^{+} and Pb^{2+}), electrostatic attraction, and surface complexation (chelation of -OH, -NH_2, -COO^{-} with Pb^{2+}). The dynamic fixed-bed adsorption capacity printed with the same material reaches 161.47 mg/g, which fits well with the Thomas model ($R^2 = 0.968$) and is suitable for continuous flow treatment; experiments show that the adsorbent performs excellently in both static oscillation and dynamic filtration, and ion strength has a slight inhibitory effect on the adsorption effect. In addition, the adsorbent can be recycled 5 times, and desorption and regeneration with hydrochloric acid are simple. Although the adsorption rate decreases in the later stage of recycling, the first adsorption efficiency is high, and the material is environmentally friendly and easy to prepare. Ma et al. [94] successfully prepared SA/CS/HNTs composite adsorbents through the "FDM 3D printing" process. The optimal addition amount of HNTs is 2 wt%. The composite material has both high specific surface area and abundant microporous structures, with excellent compressive strength and structural stability. Under optimal conditions (25℃, pH = 5.5, 250 rpm oscillation), the maximum adsorption capacity of SA + CS/HNT4 for MB is 376.3 mg/g, the adsorption rate is 80% within 60 minutes, and the removal rate reaches 99.8% within 120 minutes. The adsorption process conforms to the Langmuir monolayer adsorption model (R^2 >0.999) and pseudo-second-order kinetic model (R^2 >0.997). The adsorption mechanism of the adsorbent is mainly the electrostatic interaction between the carboxyl groups of SA, the amino groups of CS and MB, as well as the physical adsorption and hydrogen bond interaction of HNTs, which synergistically improve the adsorption performance. After 5 cycles, the composite material still maintains an adsorption rate of 64.4% and a desorption rate of 88.5%, with good regeneration performance, suitable for multiple reuse scenarios.

Geopolymers are aluminosilicate inorganic polymers formed by alkali activation of metakaolin, volcanic ash, etc. They are amorphous to semi-crystalline and consist of 3D network structures composed of silicon-oxygen tetrahedra and aluminum-oxygen tetrahedra. They adsorb heavy metals through ion exchange and surface complexation. Oliveira et al. [91] used metakaolin as a precursor, added an alkaline solution prepared by mixing sodium hydroxide and sodium silicate solutions, and then mixed with activated carbon and hydrotalcite respectively to prepare printing slurries (carried out in an ice-water bath to avoid premature polymerization). Two types of geopolymer composite adsorbents (activated carbon/hydrotalcite composite) were successfully prepared using DIW 3D printing technology. The lattice structure was designed with a porosity of 50%, and the specific surface areas were 185.6 m^2/g (3D_GP_C242) and 25.4 m^2/g (3D_GP_H), respectively. The compressive strength reaches 5.2–5.4 MPa, and the mechanical performance is better than that of freeze-dried beads samples (1.3–2.1 MPa). This material system has excellent adsorption performance: the maximum adsorption capacities of powder samples are 66.65 mg/g (P_GP_C242) and 48.82 mg/g (P_GP_H). The adsorption capacity of lattice samples is slightly lower due to mass transfer limitations, but they are easy to separate and recover; the adsorption mechanism is mainly electrostatic attraction, which conforms to the pseudo-second-order kinetic model, and the isotherm fitting is multilayer adsorption

(BET model).

Table 3 systematically summarizes the latest research progress on natural minerals and their derivatives as key functional components applied in the preparation of 3D-printed adsorbents for the remediation of water pollution. Although geopolymers are conventionally classified as polymer materials, they are essentially inorganic substances whose physical and chemical properties are much closer to those of natural minerals; therefore, they are also included and summarized in this review for a more comprehensive discussion. The abbreviations of the target pollutants investigated in the relevant studies are listed as follows: MB—Methylene Blue; SP—Suspended Particulates; UV254AOM—UV254nm Absorbing Organic Matter; CR—Congo Red; TC—Tetracycline; Rh B—Rhodamine B; MO—Methyl Orange; CECs—Contaminants of Emerging Concern (including Fluoxetine, Ketoconazole, Miconazole, Carbamazepine, etc.); CV—Crystal Violet; OMPs—Organic Micropollutants.

Table 3. Representative natural mineral-based material systems and fabrication characteristics of 3D-printed structured adsorbents for water pollution treatment

Materials	Printing Techniques	Targeted Contaminants	Adsorption Capacity	Adsorption Rate	Ref.
Zeolite Y (CBV100)	DIW	Pb^{2+}, Cu^{2+}	Pb^{2+}: 8.3 mg/g (pH = 5); Cu^{2+}: 7.8 mg/g (pH = 5)	Pb^{2+}: ≥95%; Cu^{2+}: ≥95%	[34]
Reduced GO-Loaded Zinc Oxide, Geopolymer	DIW	MB	—	95.48% (UV Irradiation for 60min Adsorption + Photocatalysis)	[92]
Montmorillonite Nanosheets	DIW	Pb^{2+}	134 mg/g (25°C, pH = 5.0, 1000 mg/L, Dosage 4 g/L)	97.58% (1st Cycle, 240 min)	[89]
Natural Clinoptilolite, Metal Oxide Composite (MgAl LDO)	DIW	MB, CR	MB: 0.17 mg/g (3D-Ze), 0.16 mg/g (3D-Ze/LDO); CR: —	MB: 98% (3D-Ze), 98% (3D-Ze/LDO); CR: 67% (3D-Ze), 79% (3D-Ze/LDO)	[93]
Geopolymer	DIW	Cs^{+}	Static Adsorption: 80.1 mg/g; Dynamic Adsorption: 21.6 mg/g	—	[94]
Zeolite A, Geopolymer	DIW	Cs^{+}	Static Adsorption: 106.3 mg/g; Dynamic Adsorption: 28.1 mg/g	—	[95]
Sodalite	DIW	Cr^{6+}	72.5 mg/g	98%	[96]
Clay (Mid Fire Cone 6 Clay), Crayfish Shell	DIW	SP, CECs	—	SP: 90.9±6.3%; CECs: 100% (Fluoxetine, Ketoconazole, Miconazole); 34% (Carbamazepine)	[97]
Graphitic Carbon Nitride (g-C_3N_4), Geopolymer, Fe^{3+} Species	DIW	MB	—	92.23% (30 min, Powder g-C_3N_4/GP (Fe)); 89.69% (60 min, 3D-g-C_3N_4/GP (Fe)+KI2)	[98]

Natural Zeolite (Clinoptilolite-Rich)	DIW	MB, CV, CR, MO	MB: 0.1363 mg/g; CV: 0.262 mg/g; CR: 0.189 mg/g; MO: Minimum (No Explicit Value)	MB: 82.5%	[99]
Metakaolin (Geopolymer Precursor)	DIW	Cs^+	21.6 mg/g	90% (Initial Concentration 300 mg/L)	[100]
Metakaolin, Activated Carbon (C242), Hydrotalcite	DIW	Orange II	41.03 mg/g (3D_GP_C242); 35.73 mg/g (3D_GP_H)	85% (P_GP_C242); 60% (P_GP_H)	[91]
Natural Zeolite (Clinoptilolite Phase)	DIW	MB	2.04 mg/g (3D-Ze/Gy50); 0.77 mg/g (3D-Ze/Gy0)	66% (3D-Ze/Gy50, pH = 10)	[101]
Metakaolin (Argical 1200S)	DIW	NH_4^+	$\geq$2.6 mg/g	$\geq$80% in the First Two Cycles (300 min)	[102]
Chabazite/4A Zeolite	DLP	Cs^+, Sr^{2+}	Cs^+: 3D-CHA: Cs/Al = 2.44, 3D-4A: Cs/Al = 1.31; Sr^{2+}: 3D-CHA: Sr/Al = 0.83, 3D-4A: Sr/Al = 0.51	—	[103]
Chitosan	DLP	MO	12.71 mg/g (BCC Structure)	90.4% (BCC Structure)	[104]
Natural Clay/Commercial Clay, Rice Husk	FDM	SP, UV254AOM	—	SP: ¿99%; UV254AOM: 67%-68%	[105]
Sodium/Potassium Aluminosilicate Zeolite (SIR-600)	FDM	NH_4^+	—	65% (Ground PLA-Zeolite Composite, Concentration 1 mg/L)	[106]
Halloysite Nanotubes, SA, Chitosan	FDM	MB	376.3 mg/g (SA+CS/HNT4, 2 wt% HNTs)	99.8% (SA+CS/HNT4, 2 wt% HNTs)	[90]
Hydroxyapatite, β-Tricalcium Phosphate	SLA	MB, TC, Rh B, MO	—	MB: 15%; TC: 18%; Rh B: 5%; MO: 3%	[107]
Polyvinylidene Fluoride Derived Porous Carbon	SLA	Bisphenol A, Phenols, Pharmaceuticals, Organic Dyes	Bisphenol A: 122.5 mg/g	Bisphenol A: 100%; Phenols: 100%; Pharmaceuticals: 100%; Organic Dyes: 100%	[108]
Hydroxyapatite	SLA	Pb^{2+}	10.4 mg/g (2.5 g Adsorbent)	98.7 $\pm$ 2.8%	[109]
Diatomite Powder	SLA	MB	0.834 mg/g (CR5ST0)	65.94% (CR5ST0)	[110]
Alumina, Natural Zeolite	SLA	NH_4^+, OMPs	NH_4^+: 0.09 mg/g	OMPs: 43% (CPC-Modified Zeolite); 41.5% (Unmodified Zeolite)	[111]

Natural zeolites are aluminosilicate minerals and porous materials that can sieve substances at the molecular scale. Currently, a large number of synthetic zeolites are also available. They have regular pores and cation exchange capacity, and are often used to adsorb ions and gases. Khalil et al. [34] mixed Y-type zeolite, nano-clay, PVA, surfactant, defoamer, and deionized water in proportion, and stirred uniformly to form a printable slurry with shear thinning characteristics. Y-type zeolite-based composite adsorbents were successfully prepared through DIW 3D printing technology. The Y-type zeolite content reaches 78.5%, and the specific surface area after calcination reaches 384 m^2/g, with typical mesoporous structure and excellent adsorption activity. Under optimal reaction conditions (pH = 5, flow rate 0.5 mL/min), the removal rates of Pb^{2+} and Cu^{2+} are both over 95%, and the treated concentrations are close to the regulatory limits for drinking water and agricultural water. The adsorption process conforms to the pseudo-second-order kinetic model. The adsorbent has good cyclic stability, and maintains structural integrity and adsorption performance after 10 adsorption-regeneration cycles. 0.5 M NaCl solution can effectively achieve desorption and regeneration. Moreover, the designed hyperboloid cylindrical structure printed achieves the self-sealing effect of columnar dynamic adsorption, suitable for continuous flow water treatment systems, and can achieve solid-liquid separation without additional filtration steps.

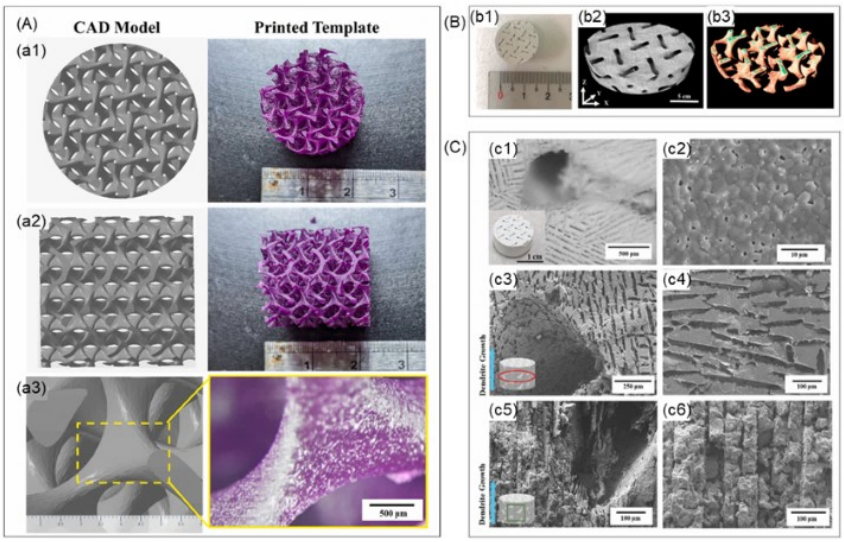

Figure 7. Topology-driven digital fabrication and multi-scale structural characterization of a gyroid-based structured scaffold

Reprinted with permission from Ref. [109] © 2024 Elsevier

Note: (A) The CAD model and 3D printed template of gyroid negative mold with topology structure in (a1) transverse view, (a2) longitudinal view, and (a3) the enlarged view; (B) the demolded scaffold and its CT scan images: (b1) The image of the gyroid structured dual-scale scaffold; the micro-CT reconstructed 3D (b2) scaffold, and (b3) macro-porosity skeleton; and (C) SEM images of the scaffold: (a) The microstructure of typical dual-scale scaffold; the FE-SEM images of (b) sintered powders, pores morphologies (c), (d) in transverse view, and (e), (f) in longitudinal view

Hydroxyapatite is a calcium phosphate salt slightly soluble in water, and is the main inorganic component of vertebrate bones and teeth. It has good biocompatibility and bioactivity, and has strong ion exchange and surface complexation capabilities for heavy metal ions (such as Pb^{2+}, Cd^{2+}). Ho et al. [109] extracted hydroxyapatite (HAp) from tilapia scales by calcination, then designed a negative mold of gyroids structure (diameter 19.5 mm, height 20 mm) through CAD, and prepared a sacrificial template by SLA 3D printing using castable wax resin (Figure 7A). Hierarchically porous HAp scaffolds were prepared by the "3D printed sacrificial template + freeze casting ice template" dual-template method. The dual-scale pore scaffolds have macro-pore diameter of 667.4 $\pm$ 95.8 μm, micro-pore diameter of 20.8 $\pm$ 5.7 μ m, and porosity of 66% (Figure 7B and C). The effective adsorption rate of the dual-scale scaffold for Pb^{2+} is 98.7 $\pm$ 2.8% with a contact time of $<$ 3 minutes; in contrast, the adsorption rate of the single-scale scaffold is 99.9 $\pm$ 0.3%, but the contact time requires 50 minutes; the adsorption mechanism of this material system is the ion exchange reaction between Ca^{2+} and Pb^{2+}. In addition, the dual-scale pore adsorbent has excellent structural performance: the permeability of the dual-scale scaffold reaches 445.6 $\pm$ 171.3 $\times 10^{-13}$ m^2, which is 30 times that of the single-scale scaffold, and the mechanical strength is 0.52 $\pm$ 0.22 MPa, with both high mass transfer efficiency and structural integrity.

Diatomite is a biogenic siliceous sedimentary rock with a lightweight and porous structure, mainly composed

of the remains of ancient diatoms, containing a small amount of clay minerals or volcanic ash, and is often used for filtration and adsorption. Li et al. [110] mixed 20 wt% diatomite powder with an aqueous solution of 2.5 wt% polyethylene oxide (PEO) and 1.5 wt% polyvinyl alcohol (PVA), and stirred uniformly to form a stable slurry as the core adsorption material system. Then, a negative mold of gyroids structure (diameter 20 mm, height 20 mm) was designed through CAD. The volume fractions of the sacrificial template were 6%, 12%, and 18%. The sacrificial template was prepared by SLA 3D printing (the resin contains wax components for easy subsequent removal). Hierarchically porous diatomite scaffolds were prepared by the "3D printed sacrificial template + freeze casting ice template" dual-template method, forming a three-level structure of "millimeter-scale spiral pores (2.36–2.82 mm) – micron-scale layered pores (8.25–13.77 μm) – nano-scale inherent pores of diatomite (430 nm)", with a porosity of 89.35%–91.44%. The optimal adsorbent sample has an adsorption rate of 65.94% for MB and an equilibrium adsorption capacity of 0.834 mg/g; the permeability of the 18% volume fraction sacrificial template sample reaches 381.36 $\times$ 10^{-12} m^2, which is 58 times that of the non-template sample, and the adsorption rate is significantly improved. In this preparation method, the volume fraction of the sacrificial template determines the millimeter-scale pore size, and the cooling rate regulates the micron-scale pore spacing; the three-level pore structure dominates the adsorption and permeability performance. The millimeter-scale pores improve mass transfer efficiency, and the nano-scale pores provide adsorption sites, greatly improving various performances of the adsorbent.

3.4 Industrial/Biological Wastes

In industry and agriculture, there are some unavoidable by-products and wastes with very large output. They themselves may not have very excellent adsorption capacity, but they have the advantage of waste utilization and local materials. There are few studies on the application of such raw materials in 3D printing adsorbents (Table 4).

Table 4. Summary of the latest research progress on the application of industrial and agricultural wastes in 3D-printed adsorbents for water pollution treatment (MB—Methylene Blue; IBU—Ibuprofen)

Materials	Printing Techniques	Targeted Contaminants	Adsorption Capacity	Adsorption Rate	Ref.
RM, Metakaolin	DIW	MB	19.96 mg/g (Langmuir, R^2=0.999)	Static: ≥99%; Dynamic: 90%	[114]
RM, Biomass Fly Ash	DIW	Pb^{2+}	—	Dynamic Adsorption: >95%	[112]
SA, Rice Husk Biochar	DIW	IBU, MB	IBU: 111.4 mg/g (Alg@Biochar10); MB: 214.6 mg/g (Alg@Biochar10)	IBU: 41%; MB: 62%	[113]
RM, Metakaolin	DIW	Cu^{2+}, Ni^{2+}, Zn^{2+}, Cd^{2+}, As^{5+}	Cu^{2+}: 3.83; Ni^{2+}: 3.72; Zn^{2+}: 3.70; Cd^{2+}: 2.78; As^{5+}: 2.39 mg/g	Cu^{2+}: 98% (Sim); 71% (AMD); Ni^{2+}: 98% (Sim); 46% (AMD); Zn^{2+}: 98% (Sim); 59% (AMD); Cd^{2+}: 97% (Sim); 72% (AMD); As^{5+}: 64% (Sim); 61% (AMD)	[115]
Sr-Doped TiO_2, Sugarcane Leaf SiO_2/Bagasse Ash	MSLA	MB	—	Sr-TiO_2/Bagasse Ash: 64.33%; Sr-TiO_2/Sugarcane Leaf SiO_2: 84.51%	[116]
Pharmaceutical Glass Waste	MSLA	MB	—	81%	[117]

For example, red mud (RM) is the main waste residue discharged after extracting alumina from bauxite. It is a typical representative of bulk industrial solid waste, rich in iron and aluminum oxides, and has strong adsorption capacity for anions (such as arsenic, phosphorus). Fly ash is fine particulate powder collected from flue gas after coal combustion in coal-fired power plants. It is formed by cooling the non-combustible mineral components brought out

by flue gas after high-temperature combustion of coal powder. It has high porosity and can be used as a precursor of geopolymers. Almeida et al. [112] pretreated RM from the aluminum industry and biomass fly ash (FA) from the biomass energy industry by grinding and sieving, mixed them with metakaolin in different proportions, and then added an alkali activator (sodium silicate: sodium hydroxide: water = 392:55.5:52.48) to adjust the liquid-solid ratio (0.60–1.01) to obtain printing ink. Geopolymer adsorbents containing high proportions of industrial wastes (up to 80 wt%, 40% RM + 40% FA) were prepared by DIW 3D printing (Figure 8). Among them, the optimal formulation (30% FA + 40% RM + 30% MK) has both high mechanical strength (26.94 MPa) and high specific surface area (40 m^2/g), with excellent water stability and no leakage of hazardous elements. The optimal printing parameters are nozzle diameter 510 μm and layer rotation angle 90°. Under these conditions, the 2-hour removal rate of Pb^{2+} by the adsorbent is >95%, and 29% is quickly removed within 15 minutes. The adsorption mechanism is the ion exchange between the negatively charged aluminosilicate network of the geopolymer and Pb^{2+}. The content of waste significantly affects the performance of the adsorbent, and the comprehensive performance is optimal when the FA content is 30%; the larger the nozzle diameter and the layer rotation angle of the printed part is 90°, the higher the mechanical strength of the adsorbent, while the specific surface area is larger (55 m^2/g) and the initial adsorption rate is faster when the layer rotation of the printed part is 45°. In addition, the adsorbent has stable performance under acidic conditions (pH = 4), suitable for acidic lead-containing wastewater treatment, and the heavy metal leakage meets environmental protection requirements, with no secondary pollution risk.

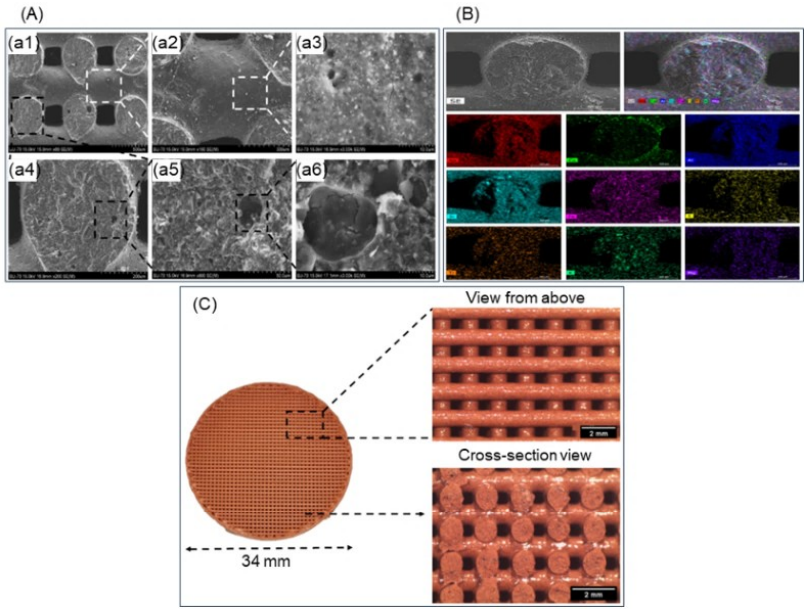

Figure 8. Multi-scale morphological and compositional characterization of a 3D-printed 30FA-based structured adsorbent

Reprinted with permission from Ref. [112] © 2024 Elsevier

Note: (A) SEM micrographs for 3D-printed 30FA with magnifications of (a1) 60×, (a2) 150×, (a3) 3000×, (a4) 200×, (a5) 800×, (a6) 3000×; (B) EDS maps (150× magnification) of the elements presents in the 30FA composition: Na, Ca, Al, Si, Fe, S, Ti, K and Mg; and (C) Optical micrographs of the 30FA structure, with magnification from the top and inner cross-section

Agricultural waste biomass, such as rice husks and sugarcane bagasse, can be directly used as cheap adsorbents, or pyrolyzed into biochar or extracted for effective components. Biochar has the characteristics of porosity, large specific surface area, and rich surface functional groups, and is a broad-spectrum adsorbent. Silva et al. [113] prepared biochar from rice husks and added it to SA water-based ink (Alg) in different proportions to obtain Alg/Biochar composite hydrogel ink. Among them, Alg/Biochar10 (10% biochar content) has the optimal performance. The adsorption capacities for IBU and MB reach 111.4 mg/g and 214.6 mg/g, respectively, which are 48% and 58% higher than those of pure SA hydrogel. The adsorption mechanisms are: IBU adsorption is mainly based on hydrogen bonds and van der Waals forces, while MB adsorption is mainly based on electrostatic attraction (negative charges on the adsorbent surface and MB cations) and π-π interactions. The adsorption process conforms to the pseudo-first-order kinetic model and Freundlich isotherm model (multilayer adsorption). It has stable performance in tap water systems, no interference from coexisting ions, can be recycled 20 times, has high desorption efficiency, and low preparation cost (about 1.06 US dollars/gram), suitable for the treatment of organic pollutants in actual water bodies, and has strong practicality.

3.5 Other Materials

In addition, some materials have been gradually applied in 3D printing adsorbents due to their unique properties (Table 5). Metal oxide nanoparticles: alumina, titanium dioxide, iron oxide, etc. These particles have large specific surface area and are often used to adsorb organic dyes, heavy metals, etc.

Table 5. Summary of the latest research progress on the application of other functional materials in 3D-printed adsorbents for water pollution treatment (MB-Methylene Blue; DCF-Diclofenac)

Materials	Printing Techniques	Targeted Contaminants	Adsorption Capacity	Adsorption Rate	Ref.
Activated Carbon Powder (Megapol 325 LS)	DIW	DCF	321 mg/g	81% (Adsorption + Electro-oxidation)	[120]
Chlorella vulgaris	FDM	Pb^{2+}	—	75.61%	[121]
Iron Particles	FDM	MB, Cu^{2+}, Hg^{2+}	—	MB: 76.61% (120 min); Cu^{2+}: 99.92% (8 h); Hg^{2+}: 100% (8 h)	[122]
Cu/Cu_2O Nanoparticles	FDM	I^- (Sim Radioactive Iodine)	4.85 mg/g	Static: 90%; Dynamic: 50%	[123]
Chlorella vulgaris	FDM	MB	33.77 mg/g (200 mg/L, 24 h, 298.15 K)	92.66% (100 mg/L, 24 h, 298.15 K)	[124]
Iron Oxide (Fe_2O_3)	FDM	As^{3+}	129.87 mg/g	Static: 95%; Dynamic Filtration: 48%	[119]
Lacunary Polyoxometalate Anions (α-$PW_9O_{34}^{9-}$)	FDM	Co^{2+}, Ni^{2+}, Cu^{2+}	—	Co^{2+}: 100% (10 Ads); 40.5% (3 Ads); Ni^{2+}: 44.2% (3 Ads); Cu^{2+}: 67.1% (3 Ads)	[125]
Titanium Dioxide NPs (TiO_2 NPs)	SLA	As^{3+}	0.922 ± 0.038 mg/g	97.38%	[118]

As magnetic particles, iron oxide can also be added to adsorbents as a magnetically driven component for magnetic recovery of adsorbents. Wang et al. [118] doped TiO_2 nanoparticles into photosensitive resin in different proportions, protected them from light with aluminum foil, and obtained composite photosensitive resin through ultrasonic dispersion and magnetic stirring. Then, TiO_2 nanoparticles were fixed on the macro face-centered cubic structure by SLA 3D printing technology. The TiO_2 nanoparticles are uniformly distributed on the surface of the printed structure (smaller particle size nanoparticles have better dispersibility) and do not lose adsorption activity due to macro molding. Among them, the 2 wt% AL5 (5–10 nm) formulation has the optimal performance. The maximum adsorption capacity for As^{3+} is 2.832 mg/g, the removal rate in pure water system reaches 99.67%, and the removal rate in groundwater treatment is 33.15%–52.87%, suitable for actual arsenic-containing wastewater treatment. The adsorption process of this material system conforms to the Freundlich isotherm model and pseudo-first-order kinetic model, mainly physical adsorption, and coexisting ions will slightly inhibit the adsorption effect. In addition, the printed adsorbent has excellent regeneration performance, maintains high adsorption activity after 10 cycles, and the desorbent NaOH is easy to obtain, with simple and efficient regeneration process. Kim et al. [119] printed filter frames of different specifications using PLA, then passed 10 M HCl solution through the channels of the PLA filter to hydrolyze polyester bonds to generate hydroxyl and carboxyl groups, improve hydrophilicity and adsorption sites, then loaded iron hydroxide on the surface of the filter, and finally prepared a PLA/iron oxide composite filtration system through pyrolysis (Figure 9 A). Among them, the 0.8 mm narrow channel specification has the optimal performance. The maximum adsorption capacity for As^{3+} is 129.87 mg/g, the static adsorption rate is 95%, and dynamic filtration can treat 950 L of arsenic-polluted water (0.01 mg/L) meeting WHO standards. Adsorption experiments found that channel width is a key parameter: the narrower the channel (0.8 mm), the larger the specific surface area (about 6.0 cm^2), the higher the iron oxide loading, and the synchronous improvement of adsorption rate and capacity. The adsorption kinetics conforms to the pseudo-second-order kinetic model ($R^2 > 0.97$). In addition, the adsorbent does not require an external power supply and relies on gravity drive. The cost of a single filter is

only 0.5 US dollars, which can be recycled 3 times. The system has strong adaptability and is suitable for on-site applications in resource-poor areas.

Activated carbon is an amorphous carbon treated by activation. As a traditional high-performance porous carbon material, it has a huge specific surface area and can remove pollutants through physical adsorption and surface chemical reactions. Acuna-Bedoya et al. [120] mixed activated carbon powder (Megapol 325 LS) with sodium carboxymethyl cellulose (CMC) to form a printable slurry, and successfully prepared an AC_m adsorption-catalysis integrated device using DIW 3D printing technology (Figure 9 B). Its BET specific surface area reaches 720 m^2/g, average pore size 0.7 nm, and good mechanical stability. It is integrated into a 3D electrode reactor (3DER) as the third electrode. It has excellent treatment effects on emerging pharmaceutical pollutants: in a single diclofenac (DCF) system, the degradation rate is 81% and the mineralization rate is 62.6% within 180 minutes; in a diclofenac-acetylsalicylic acid (DCF-ASA) mixed system, the mineralization rate is 74% within 4 hours, which is 2.5 times higher than that of the system without AC_m. Under optimal conditions (0.9 V voltage, 60 minutes adsorption), the energy consumption of this material system is 2.06 kWh/m^3, which is 50% lower than that of the system without AC_m; at the same time, the in-situ regeneration rate of AC_m after adsorption-catalysis reaches 99%, avoiding adsorbent loss and secondary pollution.

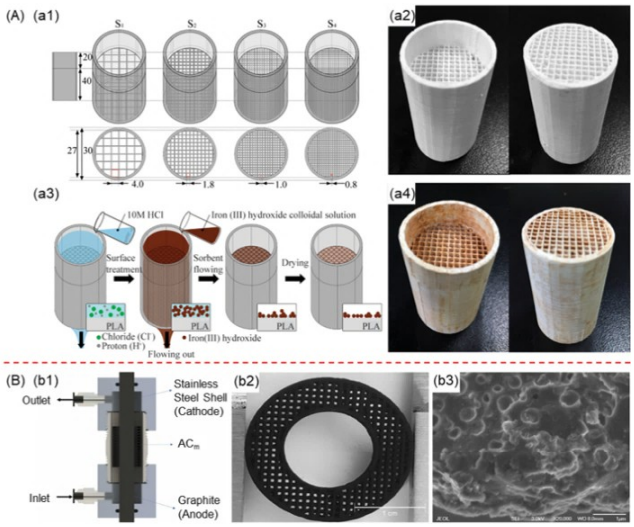

Figure 9. Digital design, fabrication, and functional integration of 3D structured filtration and electrochemical adsorption systems

Note: (A) Three-dimension filter design and illustration of sample preparation. (a1) Computer-aided designs of the filters. Four differently sized filters were designed, and the channel widths of the unit squares were 0.8, 1.0, 1.8 and 4.0 mm. All the numbers in the figure are in millimeters. (a2) Illustration of the sample preparation process on the surface of a 3D, printed PLA filter: acid hydrolysis, iron-oxide loading and drying. (a3, a4) Pictures of the top (left) and the bottom (right) of a 3D, printed filter (a3) before and (a4) after the adsorptions of iron (III) oxide; and (B) integrated 3D electrode reactor with adsorption and oxidation functions; (b1) Packed bed cell configuration; (b2) 3D-printed activated carbon electrode monolith; (b3) Its SEM image

Chlorella is a microalga and belongs to bioadsorbents. The polysaccharides, proteins and other components of its cell wall can adsorb heavy metals through complexation and ion exchange. Xia et al. [124] added different contents of Chlorella (Cp) to PLA/polybutylene adipate-terephthalate copolymer (PLA/PBAT, mass ratio 80:20), and extruded FDM printing filaments through a small blending particle wire drawing machine (155–175°C). Then, PIBCP series bio-composite adsorbents were prepared by 3D printing. Among them, PIBCP30 (30% Chlorella) has the optimal comprehensive performance. The BET adsorption conforms to the Langmuir model, the maximum adsorption capacity is 35.21 mg/g, and the adsorption is a spontaneous endothermic chemical adsorption process (pseudo-second-order kinetics, $R^2 > 0.99$). Under the conditions of 298.15 K and initial concentration 100 mg/L, the adsorption rate reaches 92.66% within 24 hours and equilibrium is reached within 800 minutes; the increase in pH and temperature is conducive to adsorption, while the increase in ion strength inhibits adsorption. In addition, the cyclic adsorption stability is good: the adsorption rate is still 72% after 6 cycles of hydrochloric acid desorption, and the mechanical strength meets the requirements of repeated use (tensile strength 22 MPa, impact strength 4 kJ/m^2).

4 From Structural Design to Performance Optimization: Strategies and Challenges

With the rapid development of 3D-printed adsorbents, the compatibility between additive manufacturing technologies and diverse material systems has been progressively enhanced. An increasing number of studies have demonstrated that, through rational structural design, appropriate material selection, and targeted post-processing strategies, 3D-printed adsorbents can achieve adsorption capacities comparable to or even exceeding those of their corresponding raw materials, while maintaining verified recyclability over multiple cycles [53, 70, 72]. From a manufacturing perspective, these improvements do not solely originate from intrinsic material properties, but rather from the synergistic optimization of geometry, multi-scale pore architecture, and post-fabrication functionalization enabled by digital fabrication technologies.

Despite these advances, current 3D-printed adsorbents still face several fundamental challenges when transitioning from laboratory demonstrations to practical deployment. In particular, limitations related to pore-scale hierarchy, long-term chemical and mechanical stability, and engineering performance under dynamic operating conditions remain significant. Addressing these issues requires a systematic understanding of how structural design and manufacturing constraints jointly influence mass transfer behavior, structural integrity, and device-level performance. The following sections therefore discuss key strategies and remaining challenges associated with hierarchical pore construction, stability for recyclability, and engineering performance evaluation in dynamic adsorption processes.

4.1 Construction of Hierarchical Pore Structures and Enhancement of Mass Transfer

Compared with conventional particulate or bulk adsorbents, 3D-printed adsorbents offer distinct advantages in terms of geometric controllability, ease of recovery, and efficient material utilization, owing to their customizable size and architecture. However, most commonly used 3D printing technologies are inherently limited to the construction of structures at the microscale level, which is several orders of magnitude larger than the micropores and mesopores that constitute the primary adsorption sites [44, 45].

This pronounced scale gap between printed microscale features and intrinsic nanoscale pores introduces complex transport phenomena during adsorption. The abrupt transition from microscale flow channels to nanoscale pores can significantly influence gas–liquid displacement behavior, interfacial stability during pore infiltration, and the morphology of the advancing liquid front. As a result, different infiltration modes, such as complete penetration or partial wetting, may occur within the adsorbent structure. These effects directly impact permeation rates and mass transfer efficiency, which at the macroscopic level manifest as variations in adsorption kinetics and the occurrence of channeling phenomena during dynamic adsorption processes [126, 127]. Such issues are further exacerbated under adsorption-dominated conditions, where relatively low fluid pressures and confining stresses prevail, making the system particularly sensitive to pore architecture.

In this context, the rational construction of hierarchical pore structures spanning micropores, mesopores, macropores, and microscale seepage channels is increasingly recognized as a critical development direction for next-generation 3D-printed adsorbents. Currently, two main strategies are employed to achieve such multi-level porosity. The first strategy involves post-printing pore-forming processes, whereby additional porosity is introduced into an initially solidified structure through physical or chemical treatments. Representative approaches include: (i) freeze-drying, which is particularly suitable for hydrogel- or biomass-based inks and generates interconnected macroporous networks through ice crystal growth and sublimation [30, 85]; (ii) sintering or pyrolysis, commonly applied to ceramic or metal slurries containing polymer binders or pore-forming agents, where the thermal removal of organic components or gas evolution during decomposition yields internally connected porous skeletons [75]; and (iii) chemical etching, which selectively removes one phase from composite materials to create additional pore networks [72].

The second strategy relies on the direct incorporation of active raw materials possessing inherent high specific surface areas and abundant micro- and mesopores-such as activated carbon powders, MOFs particles, zeolites, and highly porous biochars-into 3D printing inks as the primary functional phase [95]. This approach enables the retention of nanoscale adsorption functionality while leveraging printed microscale architectures to improve mass transfer and handling characteristics.

Advanced characterization techniques are essential for understanding and optimizing such hierarchical structures. In particular, nanoscale X-ray computed tomography (Nano-CT) enables 3D visualization of pore architectures larger than approximately 50 nm, providing valuable insights into the connectivity and spatial distribution of macropores and microscale flow channels within printed adsorbents.

4.2 Stability as the Chemical and Mechanical Foundation for Recyclability

The feasibility of recycling and reusing 3D-printed adsorbents fundamentally depends on their stability, which encompasses both chemical and mechanical aspects. Chemical stability is critical to prevent degradation of adsorption functionality and to avoid secondary pollution arising from material leaching. In most existing studies, chemical stability is indirectly assessed by comparing material characteristics before and after adsorption using techniques

such as SEM, FTIR, and XRD [34, 52, 61, 68, 71, 72]. More direct evaluations, including leaching experiments and compositional analyses following repeated adsorption cycles, have also been reported in some cases [125].

For materials with complex or poorly defined compositions—such as composites derived from multiple industrial wastes—it is strongly recommended to conduct leaching toxicity tests or targeted dissolution analyses under representative water chemistry conditions to mitigate environmental risks. For materials with well-defined compositions, in-depth surface chemical state analyses, for example using X-ray photoelectron spectroscopy (XPS), after recycling can provide valuable insights into degradation pathways and failure mechanisms at the material–solution interface.

Mechanical stability represents another critical, yet often underexplored, dimension of recyclability. At present, no unified standard exists for evaluating the mechanical robustness of 3D-printed adsorbents, and experimental protocols vary widely depending on simulated hydraulic conditions such as stirring intensity or flow-induced scouring. Moreover, different material systems exhibit distinct failure modes, including brittle fracture, plastic deformation, swelling, or structural disintegration. Consequently, many studies rely primarily on qualitative observations, for example reporting that "the structure remains intact after adsorption," which provides limited quantitative insight.

More advanced investigations have introduced quantitative mechanical assessments, including: (i) compressive strength or elastic modulus measurements, particularly suitable for monolithic structures to evaluate load-bearing capacity [41, 59, 71, 107]; and (ii) mass loss rate measurements before and after simulated flow or agitation tests to assess mechanical degradation [41, 64, 92]. From an engineering standpoint, fragmentation-induced secondary pollution poses a significant risk in environmental applications. Therefore, mechanical stability evaluation should be integrated into the early stages of material and structural design rather than deferred to later engineering validation. While comprehensive mechanical testing may not always be feasible, selecting at least one relevant and quantifiable mechanical metric tailored to the intended application scenario is strongly encouraged.

4.3 Evaluation of Engineering Performance in Dynamic Adsorption Processes

In dynamic adsorption configurations, such as fixed-bed or monolithic adsorption devices commonly referred to as filters, operational conditions are inherently more complex than those encountered in batch systems. Beyond basic stability considerations, engineering parameters including pressure drop, adsorption rate or breakthrough behavior, and optimal operating flow rates play a decisive role in determining whether an adsorption device can function efficiently with acceptable energy consumption.

Existing studies indicate that 3D-printed fixed-bed adsorption devices generally exhibit improved pressure drop characteristics compared with conventional packed powder beds [102]. Nevertheless, a high adsorption rate remains a fundamental prerequisite for effective dynamic adsorption. It should be noted that adsorption interactions vary in their binding strengths, and excessively high flow rates may lead to desorption or washout of weakly bound pollutants, thereby compromising overall removal efficiency [94].

In addition, factors such as flow channel geometry, fluid–solid friction, and structural tortuosity significantly influence the hydraulic and adsorption performance of fixed-bed devices. The ability to customize complex geometries and material compositions represents a key advantage of 3D printing; however, many existing studies remain focused on printing and shaping demonstrations without fully exploiting this capability for systematic structure–performance optimization. Even minor variations in channel design or material ratios can markedly affect adsorption behavior, rendering exhaustive experimental trial-and-error approaches impractical.

A more efficient pathway involves the integration of computational tools, such as computational fluid dynamics (CFD) simulations and data-driven optimization methods, including artificial intelligence, to screen and refine structural designs and material configurations prior to fabrication [128, 129]. Such approaches offer the potential to accelerate the development of high-performance 3D-printed adsorption devices by establishing quantitative links between digital design parameters, manufacturing constraints, and engineering performance outcomes.

5 Frontier Expansion and Paradigm Innovation

Beyond incremental improvements in adsorption performance and structural optimization, recent developments in 3D-printed adsorbents indicate the emergence of new application frontiers and manufacturing paradigms. These advances extend the role of adsorption devices from conventional pollutant removal toward risk mitigation, functional integration, and precision structural design. From a manufacturing perspective, such trends reflect a gradual shift from single-material, performance-driven fabrication toward multi-functional, architecture-driven, and paradigm-oriented design strategies. The following sections highlight several representative directions that exemplify this evolution.

5.1 Adsorption and Solidification of High-Risk Pollutants

Compared with other water treatment technologies, adsorption exhibits a distinctive advantage when recycling is not a primary concern: its inherently non-contact nature. This characteristic becomes particularly valuable when handling high-risk pollutants, where direct interaction or secondary processing may pose significant safety hazards.

Typical examples include radioactive iodine in medical wastewater, nuclear wastewater, and radioactive nuclides in nuclear-contaminated water, which present severe health risks while offering limited recycling value [130, 131].

For such pollutants, the prevailing treatment strategy involves their separation from the aqueous phase followed by solidification and long-term encapsulation. This approach has emerged as an important frontier for 3D-printed adsorbents and introduces new design requirements that extend beyond conventional adsorption metrics. In this context, adsorption devices must function not only as separation media but also as structural matrices capable of immobilizing hazardous species over extended timescales. Consequently, radiation resistance, long-term structural integrity, and reliable solidification capacity become critical performance criteria, posing substantial challenges for material selection and manufacturing strategies [62, 81, 95].

From a fabrication standpoint, these requirements call for the development of structurally robust, geometrically controllable, and chemically stable architectures that can be precisely manufactured and reliably sealed. The integration of adsorption and solidification functions within a single printed structure thus represents a paradigm shift from reversible adsorption systems toward safety-oriented, terminal containment devices.

5.2 Multi-Material Printing as a Paradigm for Resolving the Strength-Porosity Trade-Off

A long-standing challenge in the fabrication of 3D-printed adsorbents is the inherent trade-off between porosity and mechanical strength. High porosity is desirable for maximizing adsorption capacity and mass transfer efficiency; however, it often leads to compromised mechanical integrity, resulting in structural instability, fragmentation, and difficulties in recovery. Conventional solutions typically rely on empirical compromises, such as thickening printed filaments to compensate for strength loss, which in turn reduces material utilization efficiency due to limited fluid penetration.

Emerging multi-material printing technologies offer a fundamentally different strategy to address this contradiction by decoupling load-bearing and adsorption functions at the structural level. Core–shell 3D printing, for instance, employs concentric nozzles to simultaneously extrude two distinct materials at the same deposition rate, with one material encapsulating the other during printing [132, 133]. In this configuration, a mechanically robust and low-cost material can serve as the internal skeleton, while a porous, adsorption-active material forms the external shell. Mechanical strength can be tuned by adjusting the inner core diameter, without increasing the thickness of the adsorption layer, thereby avoiding unnecessary material waste.

Similarly, multi-material rotational co-extrusion printing introduces two materials through a Y-shaped flow channel into a shared nozzle, where they converge and are extruded concurrently. Owing to the high viscosity and shear-thinning behavior of the inks, the materials remain in laminar flow and form distinct layers without intermixing [134, 135]. Through controlled rotation during extrusion, the spatial distribution of skeletal and adsorption phases can be tailored, enabling enhanced structural strength or impact resistance, depending on the application scenario.

Although these advanced printing strategies have been validated in other manufacturing fields, their systematic exploration in water treatment applications remains limited. Their adoption has the potential to establish a new fabrication paradigm in which mechanical robustness and adsorption performance are no longer competing objectives but are independently optimized through architectural design.

5.3 3D Printing as a Precision Template Strategy

Prior to the advent of additive manufacturing, template-based methods were widely employed to fabricate 3D structured adsorbents [136, 137]. In contrast to conventional templates, 3D-printed templates offer substantially greater design freedom at the macroscopic scale, along with significant cost advantages for the reproducible fabrication of complex geometries.

As the spectrum of emerging pollutants continues to expand, specific adsorption based on molecular recognition is becoming increasingly important. However, many highly selective adsorption materials lack sufficient mechanical strength or processability for direct 3D printing. In such cases, the use of 3D-printed structures as precision templates, followed by physical or chemical surface modification to impart adsorption functionality, represents a promising alternative fabrication strategy [81, 109, 138].

From a manufacturing perspective, this approach enables a clear separation between structural form generation and functional material deposition. By leveraging the geometric precision of digital fabrication and the versatility of post-printing modification, adsorption performance can be tailored without sacrificing structural integrity. This template-based paradigm thus extends the role of 3D printing from a direct manufacturing tool to a versatile platform for precision structural engineering and functional integration in advanced adsorption systems.

6 Summary and Outlook: A Roadmap Towards Practical Application

6.1 Comprehensive Summary of the Review

This review systematically surveys recent progress in the development of 3D-printed structured adsorbents for water pollution treatment, with a comprehensive discussion spanning additive manufacturing technologies, material systems, structural design strategies, and performance optimization pathways. By integrating insights from materials science, advanced manufacturing, and environmental engineering, the review highlights how digital fabrication is reshaping the conceptual and practical framework of adsorption-based water treatment.

As global water pollution challenges continue to intensify in terms of pollutant diversity, concentration variability, and treatment complexity, conventional adsorbents increasingly exhibit inherent limitations, including difficult recovery, inefficient mass transfer, and insufficient mechanical robustness. Additive manufacturing, particularly 3D printing, offers a fundamentally new engineering pathway for overcoming these constraints through precise structural customization, flexible fabrication, and broad material adaptability. Accordingly, this review first categorizes and analyzes three major classes of 3D printing technologies applicable to adsorbent fabrication—material extrusion (e.g., FDM and DIW), vat photopolymerization (e.g., SLA and DLP), and powder bed fusion (e.g., SLS)—with emphasis on their respective material compatibility, fabrication resolution, and process complexity.

From the perspective of material systems, a wide range of functional materials have been successfully integrated with 3D printing technologies, including polymeric materials (e.g., chitosan and SA), advanced functional materials (e.g., metal–organic frameworks, GO, and MXene), natural minerals and their derivatives (e.g., clays, zeolites, and geopolymers), as well as industrial and biological wastes (e.g., RM and biochar). Through strategies such as compounding, filler incorporation, and post-printing functionalization, these materials can achieve efficient adsorption of heavy metals, dyes, and emerging organic pollutants while maintaining sufficient printability and demonstrating promising cyclic utilization potential.

Structural design emerges as a central factor governing the performance of 3D-printed adsorbents. This review emphasizes the construction of hierarchical pore architectures via post-processing pore-forming strategies and the use of intrinsically porous active raw materials to synergistically enhance mass transfer efficiency and adsorption capacity. In parallel, chemical and mechanical stability are identified as decisive prerequisites for practical deployment. While current studies are gradually transitioning from qualitative observations toward quantitative assessments—such as compressive strength and mass loss measurements—a universally accepted evaluation framework has yet to be established.

Regarding engineering performance in dynamic adsorption processes, 3D-printed fixed-bed and monolithic adsorption devices demonstrate clear advantages, including reduced pressure drop and simplified recovery. However, the relationship between structure and performance remains highly complex, underscoring the need for precise design and optimization approaches that integrate CFD simulations and data-driven methodologies.

Overall, additive manufacturing is driving a paradigm shift in adsorption technology, transforming adsorbents from conventional powders or granules into structurally engineered devices. Through the coordinated design of macroscopic architectures and microscopic material functionalities, 3D-printed adsorbents not only enhance adsorption performance but also significantly improve operational reliability and engineering applicability. Nevertheless, critical challenges remain, including the trade-off between porosity and mechanical strength, inconsistent performance evaluation practices, and the absence of systematic cost–benefit analyses. Addressing these issues is essential for accelerating the translation of laboratory-scale demonstrations into real-world water treatment applications.

6.2 Critical Perspectives and Future Recommendations

6.2.1 Standardization of performance evaluation and data comparability

In current literature, adsorption performance is commonly reported under optimal experimental conditions, which is effective for demonstrating material potential. However, substantial variability in parameters such as initial pollutant concentration, solution pH, and adsorbent dosage significantly limits the comparability of reported adsorption capacities across different studies.

Among these factors, the non-standardized and sometimes ambiguous reporting of adsorbent dosage represents a particularly critical issue. Adsorbent dosage, typically expressed as the mass-to-volume ratio (m/V), directly governs the effective adsorbent–pollutant ratio and exerts a decisive influence on the apparent adsorption capacity. Nevertheless, existing studies frequently exhibit inconsistent dosage selection within the same work, employ vague descriptors such as “pieces,” or omit the rationale for dosage determination altogether. Such practices undermine data reproducibility and hinder meaningful comparison.

Fundamentally, for materials exhibiting complex adsorption mechanisms involving both physical and chemical interactions, apparent adsorption capacity is intrinsically dosage-dependent. Under non-saturated conditions, variations in dosage alter the equilibrium pollutant concentration, thereby influencing adsorption outcomes. Consequently, discussing adsorption capacity in isolation from dosage parameters can be misleading.

Although accurately determining wet mass for certain materials, such as hydrogels, presents technical challenges, this further underscores the urgency of establishing clear and reproducible experimental and reporting standards. Future studies are therefore encouraged to: (1) uniformly and explicitly report all key experimental parameters, particularly adsorbent dosage using standardized units (e.g., g/L or mg/mL); (2) interpret adsorption performance in conjunction with adsorption isotherms, kinetics, and dosage-dependent behavior rather than relying solely on single optimal values; and (3) clearly justify dosage selection based on preliminary experiments or realistic application scenarios.

6.2.2 Life-cycle cost considerations and sustainability-oriented design

A traditional advantage of adsorption lies in its potential cost-effectiveness and operational simplicity. However, in the context of 3D-printed adsorbents, high adsorption performance is often pursued through complex pre-processing steps, energy-intensive printing technologies, or elaborate post-treatment procedures. While such approaches can enhance material performance and structural precision, they also increase fabrication complexity and economic cost, potentially conflicting with the fundamental appeal of adsorption as a simple and economical treatment method.

Importantly, the core value proposition of 3D-printed adsorbents resides not merely in material-level performance but in system-level engineering advantages—such as high flux, low pressure drop, and simplified recovery—that are difficult to achieve with conventional powder or granular adsorbents. From a life-cycle perspective, a reusable monolithic adsorbent that eliminates repeated solid–liquid separation steps may ultimately offer lower operational costs than disposable particulate materials.

Accordingly, comparisons based solely on preparation cost at the laboratory stage are often insufficient and potentially misleading. Future research should emphasize the integrated design of performance, cost, and sustainability by promoting the use of low-value or waste-derived raw materials, simplified fabrication routes, and mild processing conditions. Advancing from performance-driven demonstrations toward application-oriented optimization is essential for enabling engineering translation.

Furthermore, as an environmentally motivated research field, the ecological footprint associated with material selection, energy consumption, and by-product generation during the entire fabrication process should be explicitly considered. The adoption of environmentally benign materials and the valorization of industrial and agricultural wastes merit continued emphasis.

6.2.3 Interdisciplinary integration and intelligent design paradigms

Research on 3D-printed adsorbents is inherently interdisciplinary, bridging materials science, environmental engineering, advanced manufacturing, and fluid mechanics. Future breakthroughs are likely to depend on a fundamental shift from empirical trial-and-error approaches toward data-driven, simulation-first, and intelligently controlled manufacturing paradigms, necessitating deeper integration with computational sciences.

At the material and process optimization level, machine learning and artificial intelligence offer transformative opportunities. The compatibility between adsorbent materials and binders, as well as subtle variations in printing parameters such as extrusion pressure, printing speed, and layer thickness, can exert complex and coupled effects on structural fidelity, pore architecture, and final performance. Emerging studies have demonstrated the feasibility of predicting adsorption isotherm behavior and maximum adsorption capacity based solely on material composition and preparation parameters, pointing toward a future in which reverse design becomes possible. By constructing high-quality experimental databases and leveraging artificial intelligence algorithms to uncover hidden correlations among material, process, structure, and performance, optimal formulations and printing conditions can be intelligently recommended according to target treatment requirements.

At the device and system level, computational tools are transitioning from optional aids to essential components of the design workflow. As 3D printing evolves from producing simple adsorption blocks to fabricating integrated adsorption devices and reactors with complex internal flow architectures, traditional experimental fluid dynamics approaches become increasingly inefficient. CFD simulations enable the prediction and optimization of flow distribution, mass transfer efficiency, pressure drop, and channeling resistance for various channel geometries prior to fabrication. This "simulation–screening–printing–validation" cycle allows the theoretical freedom of digital design to be translated into tangible performance gains.

Beyond these aspects, intelligent manufacturing paradigms facilitate broader interdisciplinary integration. Potential directions include coupling adsorption structures with catalytic or oxidative functionalities through multi-material printing to realize adsorption–degradation synergy, embedding conductive sensing elements to develop intelligent adsorbents capable of real-time monitoring, and integrating life-cycle assessment tools at the digital design stage to guide sustainable manufacturing decisions.

In conclusion, future research on 3D-printed adsorbents should transcend isolated material modification and simplistic geometric replication. The long-term vision entails completing the entire virtual-to-physical workflow within a digital environment—from molecular-scale active site design and macro–micro structural topology optimization to system-level hydraulic performance prediction via multi-physics simulation and artificial intelligence—followed

by accurate materialization of the optimized design through advanced multi-material and multi-scale additive manufacturing. Embracing this paradigm will enable 3D-printed adsorbents to evolve from an emerging fabrication technique into a central technological engine driving the next generation of water treatment solutions.

Author Contributions

Conceptualization, T.H.D. and L.Z.; methodology, T.H.D.; investigation, T.H.D.; resources, T.H.D.; data curation, T.H.D.; writing—original draft preparation, T.H.D.; writing—review and editing, T.H.D.; supervision, L.Z. All authors have read and agreed to the published version of the manuscript.

Data Availability

The data used to support the research findings are available from the corresponding author upon request.

Conflicts of Interest

The authors declare no conflict of interest.

References

[1] R. P. Schwarzenbach, T. Egli, T. B. Hofstetter, U. von Gunten, and B. Wehrli, "Global water pollution and human health," *Annu. Rev. Environ. Resour.*, vol. 35, pp. 109–136, 2010. https://doi.org/10.1146/annurev-environ-100809-125342

[2] G. Crini and E. Lichtfouse, "Advantages and disadvantages of techniques used for wastewater treatment," *Environ. Chem. Lett.*, vol. 17, no. 1, pp. 145–155, 2019. https://doi.org/10.1007/s10311-018-0785-9

[3] R. Al-Tohamy, S. S. Ali, F. H. Li, K. M. Okasha, Y. A. G. Mahmoud, T. Elsamahy, H. X. Jiao, Y. Y. Fu, and J. Z. Sun, "A critical review on the treatment of dye-containing wastewater: Ecotoxicological and health concerns of textile dyes and possible remediation approaches for environmental safety," *Ecotoxicol. Environ. Saf.*, vol. 231, p. 113160, 2022. https://doi.org/10.1016/j.ecoenv.2021.113160

[4] N. A. A. Qasem, R. H. Mohammed, and D. U. Lawal, "Removal of heavy metal ions from wastewater: A comprehensive and critical review," *npj Clean Water*, vol. 4, no. 1, p. 36, 2021. https://doi.org/10.1038/s41545-021-00127-0

[5] A. A. Koelmans, N. H. M. Nor, E. Hermsen, M. Kooi, S. M. Mintenig, and J. De France, "Microplastics in freshwaters and drinking water: Critical review and assessment of data quality," *Water Res.*, vol. 155, pp. 410–422, 2019. https://doi.org/10.1016/j.watres.2019.02.054

[6] C. Y. Teh, P. M. Budiman, K. P. Y. Shak, and T. Y. Wu, "Recent advancement of coagulation-flocculation and its application in wastewater treatment," *Ind. Eng. Chem. Res.*, vol. 55, no. 16, pp. 4363–4389, 2016. https://doi.org/10.1021/acs.iecr.5b04703

[7] D. B. Miklos, C. Remy, M. Jekel, K. G. Linden, J. E. Drewes, and U. Hübner, "Evaluation of advanced oxidation processes for water and wastewater treatment—A critical review," *Water Res.*, vol. 139, pp. 118–131, 2018. https://doi.org/10.1016/j.watres.2018.03.042

[8] E. O. Ezugbe and S. Rathilal, "Membrane technologies in wastewater treatment: A review," *Membranes*, vol. 10, no. 5, p. 89, 2020. https://doi.org/10.3390/membranes10050089

[9] G. P. Sheng, H. Q. Yu, and X. Y. Li, "Extracellular polymeric substances (EPS) of microbial aggregates in biological wastewater treatment systems: A review," *Biotechnol. Adv.*, vol. 28, no. 6, pp. 882–894, 2010. https://doi.org/10.1016/j.biotechadv.2010.08.001

[10] G. Crini, E. Lichtfouse, L. D. Wilson, and N. Morin-Crini, "Conventional and non-conventional adsorbents for wastewater treatment," *Environ. Chem. Lett.*, vol. 17, no. 1, pp. 195–213, 2019. https://doi.org/10.1007/s10311-018-0786-8

[11] H. N. Tran, S. J. You, A. Hosseini-Bandegharaei, and H. P. Chao, "Mistakes and inconsistencies regarding adsorption of contaminants from aqueous solutions: A critical review," *Water Res.*, vol. 120, pp. 88–116, 2017. https://doi.org/10.1016/j.watres.2017.04.014

[12] W. Gao, Y. B. Zhang, D. Ramanujan, K. Ramani, Y. Chen, C. B. Williams, C. C. L. Wang, Y. C. Shin, S. Zhang, and P. D. Zavattieri, "The status, challenges, and future of additive manufacturing in engineering," *Comput. Aided Des.*, vol. 69, pp. 65–89, 2015. https://doi.org/10.1016/j.cad.2015.04.001

[13] T. D. Ngo, A. Kashani, G. Imbalzano, K. T. Q. Nguyen, and D. Hui, "Additive manufacturing (3D printing): A review of materials, methods, applications and challenges," *Compos. Part B: Eng.*, vol. 143, pp. 172–196, 2018. https://doi.org/10.1016/j.compositesb.2018.02.012

[14] M. N. Nadagouda, M. Ginn, and V. Rastogi, "A review of 3D printing techniques for environmental applications," *Curr. Opin. Chem. Eng.*, vol. 28, pp. 173–178, 2020. https://doi.org/10.1016/j.coche.2020.08.002

[15] A. P. Fagundes, J. O. D. Lira, N. Padoin, C. Soares, and H. G. Riella, "Additive manufacturing of functional devices for environmental applications: A review," *J. Environ. Chem. Eng.*, vol. 10, no. 3, p. 108049, 2022. https://doi.org/10.1016/j.jece.2022.108049

[16] Y. F. Zhang, J. Z. Li, Y. Zou, Y. L. Liu, L. Li, J. H. Xu, D. Li, Q. Q. Rong, J. Y. Li, and Y. X. Geng, "3D printing technologies in water treatment: Applications, challenges, and emerging trends," *Chem. Eng. J.*, vol. 500, p. 157184, 2024. https://doi.org/10.1016/j.cej.2024.157184

[17] D. Lopez-Rodriguez, B. Mico-Vicent, J. Jordan-Nunez, M. Bonet-Aracil, and E. Bou-Belda, "Uses of Nanoclays and adsorbents for dye recovery: A textile industry review," *Appl. Sci.-Basel*, vol. 11, no. 23, p. 11422, 2021. https://doi.org/10.3390/app112311422

[18] S. Mallakpour, E. Azadi, and C. M. Hussain, "MOF/COF-based materials using 3D printing technology: Applications in water treatment, gas removal, biomedical, and electronic industries," *New J. Chem.*, vol. 45, no. 30, pp. 13 247–13 257, 2021. https://doi.org/10.1039/d1nj02152d

[19] N. H. M. Yusoff, L. R. I. Teo, S. J. Phang, V. L. Wong, K. H. Cheah, and S. S. Lim, "Recent Advances in polymer-based 3D printing for wastewater treatment application: An overview," *Chem. Eng. J.*, vol. 429, p. 132311, 2022. https://doi.org/10.1016/j.cej.2021.132311

[20] W. E. King, A. T. Anderson, R. M. Ferencz, N. E. Hodge, C. Kamath, S. A. Khairallah, and A. M. Rubenchik, "Laser powder bed fusion additive manufacturing of metals; physics, computational, and materials challenges," *Appl. Phys. Rev.*, vol. 2, no. 4, p. 041304, 2015. https://doi.org/10.1063/1.4937809

[21] M. Ziaee and N. B. Crane, "Binder jetting: A review of process, materials, and methods," *Addit. Manuf.*, vol. 28, pp. 781–801, 2019. https://doi.org/10.1016/j.addma.2019.05.031

[22] D. Svetlizky, M. Das, B. L. Zheng, A. L. Vyatskikh, S. Bose, A. Bandyopadhyay, J. M. Schoenung, E. J. Lavernia, and N. Eliaz, "Directed energy deposition (DED) additive manufacturing: Physical characteristics, defects, challenges and applications," *Mater. Today*, vol. 49, pp. 271–295, 2021. https://doi.org/10.1016/j.mattod.2021.03.020

[23] Y. L. Tee, P. Tran, M. Leary, P. Pille, and M. Brandt, "3D printing of polymer composites with material jetting: Mechanical and fractographic analysis," *Addit. Manuf.*, vol. 36, p. 101558, 2020. https://doi.org/10.1016/j.addma.2020.101558

[24] J. Gonzalez-Gutierrez, S. Cano, S. Schuschnigg, C. Kukla, J. Sapkota, and C. Holzer, "Additive manufacturing of metallic and ceramic components by the material extrusion of highly-filled polymers: A review and future perspectives," *Materials*, vol. 11, no. 5, p. 840, 2018. https://doi.org/10.3390/ma11050840

[25] P. M. Bhatt, A. M. Kabir, M. Peralta, H. A. Bruck, and S. K. Gupta, "A robotic cell for performing sheet lamination-based additive manufacturing," *Addit. Manuf.*, vol. 27, pp. 278–289, 2019. https://doi.org/10.1016/j.addma.2019.02.002

[26] F. Zhang, L. Y. Zhu, Z. A. Li, S. Y. Wang, J. P. Shi, W. L. Tang, N. Li, and J. Q. Yang, "The recent development of vat photopolymerization: A review," *Addit. Manuf.*, vol. 48, p. 102423, 2021. https://doi.org/10.1016/j.addma.2021.102423

[27] S. Wickramasinghe, T. Do, and P. Tran, "FDM-based 3D printing of polymer and associated composite: A review on mechanical properties, defects and treatments," *Polymers*, vol. 12, no. 7, p. 1529, 2020. https://doi.org/10.3390/polym12071529

[28] S. Singh, S. Ramakrishna, and R. Singh, "Material issues in additive manufacturing: A review," *J. Manuf. Process.*, vol. 25, pp. 185–200, 2017. https://doi.org/10.1016/j.jmapro.2016.11.006

[29] H. Rezaei, A. A. Matin, S. Vahdati-khajeh, and B. Habibi, "3D printed solid phase microextraction scaffolds as novel tool for sample preparation; application in antifungal drugs analysis," *J. Chromatogr. B*, vol. 1225, p. 123757, 2023. https://doi.org/10.1016/j.jchromb.2023.123757

[30] Y. S. Wang, Y. Wang, S. Qiu, C. Y. Wang, H. Zhang, J. Guo, S. F. Wang, and H. X. Ma, "3D-printed filters for efficient heavy metal removal from water using pla@cs/hap composites," *Polymers*, vol. 15, no. 20, p. 4144, 2023. https://doi.org/10.3390/polym15204144

[31] I. L. Liakos, A. Mondini, E. Del Dottore, C. Filippeschi, F. Pignatelli, and B. Mazzolai, "3D printed composites from heat extruded polycaprolactone/sodium alginate filaments and their heavy metal adsorption properties," *Mater. Chem. Front.*, vol. 4, no. 8, pp. 2472–2483, 2020. https://doi.org/10.1039/d0qm00159g

[32] M. Saadi, A. Maguire, N. T. Pottackal, M. S. H. Thakur, M. M. Ikram, A. J. Hart, P. M. Ajayan, and M. M. Rahman, "Direct ink writing: A 3D printing technology for diverse materials," *Adv. Mater.*, vol. 34, no. 28, p. 2108855, 2022. https://doi.org/10.1002/adma.202108855

[33] J. A. Lewis, "Direct ink writing of 3D functional materials," *Adv. Funct. Mater.*, vol. 16, no. 17, pp. 2193–2204, 2006. https://doi.org/10.1002/adfm.200600434

[34] A. Khalil, R. Hashaikeh, and N. Hilal, "3D printed zeolite-y for removing heavy metals from water," *J. Water Process Eng.*, vol. 42, p. 102187, 2021. https://doi.org/10.1016/j.jwpe.2021.102187

[35] J. G. Huang, Q. Qin, and J. Wang, "A review of stereolithography: Processes and systems," *Processes*, vol. 8, no. 9, p. 1138, 2020. https://doi.org/10.3390/pr8091138

[36] G. Zhou, Q. Y. Han, J. Tai, B. B. Liu, J. Zhang, K. P. Wang, X. Ni, P. P. Wang, X. C. Liu, and A. X. Jiao, "Digital light procession three-dimensional printing acrylate/collagen composite airway stent for tracheomalacia," *J. Bioact. Compat. Polym.*, vol. 32, no. 4, pp. 429–442, 2017. https://doi.org/10.1177/0883911516686090

[37] M. Staffová, F. Ondreás, J. Svatík, M. Zboncák, J. Jancár, and P. Lepcio, "3D printing and post-curing optimization of photopolymerized structures: Basic concepts and effective tools for improved thermomechanical properties," *Polym. Test.*, vol. 108, p. 107499, 2022. https://doi.org/10.1016/j.polymertesting.2022.107499

[38] C. Zhou, Y. Chen, Z. G. Yang, and B. Khoshnevis, "Digital material fabrication using mask-image-projection-based stereolithography," *Rapid Prototyp. J.*, vol. 19, no. 3, pp. 153–165, 2013. https://doi.org/10.1108/13552541311312148

[39] F. Ranjbar, A. M. Rezadoust, S. Sadjadi, and M. Atai, "3D-printed cyclodextrin polymer-g-c_3n_4 nanocomposite as a monolithic adsorbent for dye removal," *Prog. Addit. Manuf.*, vol. 11, no. 1, pp. 1317–1340, 2026. https://doi.org/10.1007/s40964-025-01413-w

[40] T. Wu, N. Zare, Y. Li, D. X. Zhang, E. N. Dragoi, T. M. Aminabhavi, and H. Karimi-Maleh, "3D printed monolithic adsorbent for removal of Congo red and silver ions: Batch and fixed bed column studies," *Chem. Eng. J.*, vol. 519, p. 164865, 2025. https://doi.org/10.1016/j.cej.2025.164865

[41] M. Y. N. Husna, C. H. Chong, V. L. Wong, K. H. Cheah, and Y. K. Wan, "3D-printed PEGDA monolith with robust silane-grafted chitosan for enhanced textile wastewater treatment," *J. Environ. Chem. Eng.*, vol. 10, no. 6, p. 108581, 2022. https://doi.org/10.1016/j.jece.2022.108581

[42] J. P. Kruth, X. Wang, T. Laoui, and L. Froyen, "Lasers and materials in selective laser sintering," *Assem. Autom.*, vol. 23, no. 4, pp. 357–371, 2003. https://doi.org/10.1108/01445150310698652

[43] M. A. Al-Ghouti and D. A. Da'ana, "Guidelines for the use and interpretation of adsorption isotherm models: A review," *J. Hazard. Mater.*, vol. 393, p. 122383, 2020. https://doi.org/10.1016/j.jhazmat.2020.122383

[44] J. L. Wang and X. Guo, "Adsorption kinetic models: Physical meanings, applications, and solving methods," *J. Hazard. Mater.*, vol. 390, p. 122156, 2020. https://doi.org/10.1016/j.jhazmat.2020.122156

[45] J. P. Vareda, "On validity, physical meaning, mechanism insights and regression of adsorption kinetic models," *J. Mol. Liquids*, vol. 376, p. 121416, 2023. https://doi.org/10.1016/j.molliq.2023.121416

[46] S. B. Wang and Y. L. Peng, "Natural zeolites as effective adsorbents in water and wastewater treatment," *Chem. Eng. J.*, vol. 156, no. 1, pp. 11–24, 2010. https://doi.org/10.1016/j.cej.2009.10.029

[47] M. K. Uddin, "A review on the adsorption of heavy metals by clay minerals, with special focus on the past decade," *Chem. Eng. J.*, vol. 308, pp. 438–462, 2017. https://doi.org/10.1016/j.cej.2016.09.029

[48] A. Alsbaiee, B. J. Smith, L. L. Xiao, Y. H. Ling, D. E. Helbling, and W. R. Dichtel, "Rapid removal of organic micropollutants from water by a porous $beta$-cyclodextrin polymer," *Nature*, vol. 529, no. 7585, pp. 190–U146, 2016. https://doi.org/10.1038/nature16185

[49] G. Crini, "Non-conventional low-cost adsorbents for dye removal: A review," *Bioresour. Technol.*, vol. 97, no. 9, pp. 1061–1085, 2006. https://doi.org/10.1016/j.biortech.2005.05.001

[50] G. A. Appuhamillage, D. R. Berry, C. E. Benjamin, M. A. Luzuriaga, J. C. Reagan, J. J. Gassensmith, and R. A. Smaldone, "A biopolymer-based 3D printable hydrogel for toxic metal adsorption from water," *Polym. Int.*, vol. 68, no. 5, pp. 964–971, 2019. https://doi.org/10.1002/pi.5787

[51] Y. Wu, C. X. Tang, P. X. Si, and D. Zhang, "3D coaxial printing of porous construct stacked with hollow filaments for heavy metal removal," *Sci. Total Environ.*, vol. 887, p. 164120, 2023. https://doi.org/10.1016/j.scitotenv.2023.164120

[52] S. Fuxiang, W. Na, Z. Qiangqiang, W. B. Jie, and L. Bin, "3D printing calcium alginate adsorbents for highly efficient recovery of U (VI) in acidic conditions," *J. Hazard. Mater.*, vol. 440, p. 129774, 2022. https://doi.org/10.1016/j.jhazmat.2022.129774

[53] M. Shahbazi, H. Jäger, S. J. Ahmadi, and M. Lacroix, "Electron beam crosslinking of alginate/nanoclay ink to improve functional properties of 3D printed hydrogel for removing heavy metal ions," *Carbohydr. Polym.*, vol. 240, p. 116211, 2020. https://doi.org/10.1016/j.carbpol.2020.116211

[54] Z. X. Liu, X. T. Zhou, and C. J. Liu, "N-doped porous carbon material prepared via direct ink writing for the removal of methylene blue," *Diamond Relat. Mater.*, vol. 95, pp. 121–126, 2019. https://doi.org/10.1016/j.diamond.2019.04.010

[55] C. Noè, A. Cosola, A. Chiappone, M. Hakkarainen, H. Grützmacher, and M. Sangermano, "From polysaccharides to UV-curable biorenewable organo/hydrogels for methylene blue removal," *Polymers*, vol. 235, p. 124257, 2021. https://doi.org/10.1016/j.polymer.2021.124257

[56] L. A. Lagalante, A. J. Lagalante, and A. F. Lagalante, "3D printed solid-phase extraction sorbents for removal of volatile organic compounds from water," *J. Water Process Eng.*, vol. 35, p. 101194, 2020. https://doi.org/10.1016/j.jwpe.2020.101194

[57] A. F. Kanaan and A. P. Piedade, "3D printing and blue sustainability: Taking advantage of process-induced defects for the metallic ion removal from water," *Polymers*, vol. 16, no. 14, p. 1992, 2024. https://doi.org/10.3390/polym16141992

[58] P. A. Kashi, A. Mohammadi, J. S. Chen, R. Ettelaie, H. Jager, and M. Shahbazi, "3D printing of a photo-curable hydrogel to engineer mechanically robust porous structure for ion capture or sustained potassium ferrate (vi) release for water treatment," *Sep. Purif. Technol.*, vol. 344, p. 127247, 2024. https://doi.org/10.1016/j.seppur.2024.127247

[59] S. Graziosi, S. Badini, C. Lammi, C. Bollati, S. Regondi, and R. Pugliese, "Biocompatible and soft micro/nanoporous 3D-printed scaffolds with superoleophilic/superadsorption capabilities," *Appl. Mater. Today*, vol. 45, p. 102853, 2025. https://doi.org/10.1016/j.apmt.2025.102853

[60] Z. Liu, X. S. Xia, W. Li, L. R. Xiao, X. L. Sun, F. B. Luo, Q. H. Chen, and Q. R. Qian, "In Situ growth of ca^{2+}-based metal-organic framework on $casio_3$/abs/tpu 3D skeleton for methylene blue removal," *Materials*, vol. 13, no. 19, p. 4403, 2020. https://doi.org/10.3390/ma13194403

[61] T. S. Ng, A. Norman, N. H. M. Yusoff, C. H. Chong, K. H. Cheah, T. C. Yap, and V. L. Wong, "3D printing and optimization of biocompatible and hydrophilic PEGDA-HEMA lattice for enhanced RhB dye removal from aqueous solution," *Int. J. Polym. Sci.*, vol. 2024, p. 6633503, 2024. https://doi.org/10.1155/2024/6633503

[62] J. M. Li, P. Gao, N. Li, and Z. N. Wang, "3D-printed amidoximed hollow spheres with enhanced selectivity and antifouling property for uranium recovery from wastewater," *Desalination Water Treat.*, vol. 289, pp. 111–122, 2023. https://doi.org/10.5004/dwt.2023.29377

[63] G. T. X. Yong, W. B. Koh, N. Yusoff, A. Norman, C. H. Chong, K. H. Cheah, and V. L. Wong, "3D-printed SiOC ceramics grafted with chitosan-graphene oxide composite for enhanced dye adsorption," *Sep. Purif. Technol.*, vol. 362, p. 131669, 2025. https://doi.org/10.1016/j.seppur.2025.131669

[64] N. H. M. Yusoff, L. Loh, C. H. Chong, V. L. Wong, K. H. Cheah, and Y. K. Wan, "Electron beam-induced surface modification on nanochitosan-grafted 3D-printed monoliths for enhanced wastewater color removal," *Int. J. Chem. Eng.*, vol. 2025, no. 1, p. 2199479, 2025. https://doi.org/10.1155/ijce/2199479

[65] D. X. Zhang, J. F. Xiao, Q. Q. Guo, and J. Yang, "3D-printed highly porous and reusable chitosan monoliths for Cu(II) removal," *J. Mater. Sci.*, vol. 54, no. 8, pp. 6728–6741, 2019. https://doi.org/10.1007/s10853-019-03332-y

[66] L. Shahzadi, F. Maya, M. C. Breadmore, and S. C. Thickett, "Thiol-yne 3D printable polymeric resins for the efficient removal of a model pollutant from waters," *Macromol. Mater. Eng.*, vol. 308, no. 4, 2023. https://doi.org/10.1002/mame.202200497

[67] S. Kulomäki, E. Lahtinen, S. Perämäki, and A. Väisänen, "Preconcentration and speciation analysis of mercury: 3D printed metal scavenger-based solid-phase extraction followed by analysis with inductively coupled plasma mass spectrometry," *Talanta*, vol. 240, p. 123163, 2022. https://doi.org/10.1016/j.talanta.2021.123163

[68] J. Frimodig, A. Autio, E. Lahtinen, and M. Haukka, "Recovery of $17beta$-estradiol using 3D printed polyamide-12 scavengers," *3D Print. Addit. Manuf.*, vol. 10, no. 5, pp. 1122–1129, 2023. https://doi.org/10.1089/3dp.2021.0063

[69] T. Wu, Y. Li, Z. X. Zhang, D. X. Zhang, E. N. Dragoi, and H. Karimi-Maleh, "3D print-based polypyrrole/TiVCTx/UiO-66 composites for effective adsorption of combined pollutants in water media," *J. Nanostruct. Chem.*, vol. 15, no. 1, p. 152503, 2025. https://doi.org/10.57647/jnsc.2025.1501.03

[70] R. Pei, L. L. Fan, F. G. Zhao, J. R. Xiao, Y. C. Yang, A. N. Lai, S. F. Zhou, and G. W. Zhan, "3D-printed metal-organic frameworks within biocompatible polymers as excellent adsorbents for organic dyes removal," *J. Hazard. Mater.*, vol. 384, p. 121418, 2020. https://doi.org/10.1016/j.jhazmat.2019.121418

[71] X. H. Liu, S. J. Zhao, Q. H. Li, P. G. He, X. M. Duan, D. C. Jia, and Y. Zhou, "3D printed GO-g-C3N4-geopolymer components with acid treatment for the removal of methylene blue from wastewater," *J. Am. Ceram. Soc.*, vol. 108, no. 5, 2025. https://doi.org/10.1111/jace.20377

[72] H. N. Zhang, W. H. Niu, X. M. Liu, J. P. Han, Y. Zhao, Z. Q. Wei, Z. G. Wu, Z. Y. Shi, B. X. Wang, and Y. K. Dong, "3D printing of antimicrobial adsorbents using mercapto-graphene oxide/chitosan/ϵ-polylysine: Elucidating adsorption mechanisms and antimicrobial performance," *Int. J. Biol. Macromol.*, vol. 283, 2024. https://doi.org/10.1016/j.ijbiomac.2024.137797

[73] D. S. Liu, P. Jiang, X. C. Li, J. X. Liu, L. C. Zhou, X. L. Wang, and F. Zhou, "3D printing of metal-organic frameworks decorated hierarchical porous ceramics for high-efficiency catalytic degradation," *Chem. Eng. J.*, vol. 397, 2020. https://doi.org/10.1016/j.cej.2020.125392

[74] H. N. Zhang, X. M. Liu, J. P. Han, W. H. Niu, B. X. Wang, Z. G. Wu, Z. Q. Wei, Y. Zhu, Q. Guo, and X. L.

Wang, "Acid-resistant chitosan/graphene oxide adsorbent for Cu^{2+} removal: The role of mixed cross-linking and amino-functionalized," *Int. J. Biol. Macromol.*, vol. 273, 2024. https://doi.org/10.1016/j.ijbiomac.2024.133096

[75] S. Q. Ma, X. H. Liu, S. Fu, S. J. Zhao, P. G. He, X. M. Duan, Z. H. Yang, D. C. Jia, P. Colombo, and Y. Zhou, "Direct ink writing of porous SiC ceramics with geopolymer as binder," *J. Eur. Ceram. Soc.*, vol. 42, no. 15, pp. 6815–6826, 2022. https://doi.org/10.1016/j.jeurceramsoc.2022.08.004

[76] A. Masud, C. Zhou, and N. Aich, "Emerging investigator series: 3D printed graphene-biopolymer aerogels for water contaminant removal: A proof of concept," *Environ. Sci.-Nano*, vol. 8, no. 2, 2021. https://doi.org/10.1039/D0EN00953A

[77] N. Wang, Y. Xu, Y. Y. Wei, Q. Chen, F. X. Song, and B. Liu, "Proportion-optimized 3D-printed calcium alginate/graphene oxide adsorbent for efficient uranium separation from aqueous solutions," *Sep. Purif. Technol.*, vol. 377, 2025. https://doi.org/10.1016/j.seppur.2025.134199

[78] H. S. Far, M. Najafi, M. Hasanzadeh, and R. Rahimi, "A 3D-printed hierarchical porous architecture of MOF@clay composite for rapid and highly efficient dye scavenging," *New J. Chem.*, vol. 46, no. 48, pp. 23 351–23 360, 2022. https://doi.org/10.1039/D2NJ05188E

[79] S. J. Phang, V. L. Wong, K. H. Cheah, and L. L. Tan, "Robust graphitic carbon nitrite-based thermoset coating for synergistic adsorption-photocatalysis process in 3D-printed photoreactors," *Energy Rep.*, vol. 9, pp. 30–37, 2023. https://doi.org/10.1016/j.egyr.2022.11.159

[80] H. S. Far, M. Najafi, M. Hasanzadeh, and M. Rabbani, "Self-supported 3D-printed lattices containing MXene/metal-organic framework (MXOF) composite as an efficient adsorbent for wastewater treatment," *ACS Appl. Mater. Interfaces*, vol. 14, no. 39, pp. 44 488–44 497, 2022. https://doi.org/10.1021/acsami.2c13830

[81] M. del Rio, M. Villar, S. Quesada, G. T. Palomino, L. Ferrer, and C. P. Cabello, "Silver-functionalized UiO-66 metal-organic framework-coated 3D printed device for the removal of radioactive iodine from wastewaters," *Appl. Mater. Today*, vol. 24, 2021. https://doi.org/10.1016/j.apmt.2021.101130

[82] K. Li, Y. D. de Miménand, X. Y. Jin, J. G. Yi, and J. Guo, "Metal Oxide (ZnO and TiO2) and Fe-based metal-organic framework nanoparticles on 3D-printed fractal polymer surfaces for photocatalytic degradation of organic pollutants," *ACS Appl. Nano Mater.*, vol. 3, no. 3, pp. 2830–2845, 2020. https://doi.org/10.1021/acsanm.0c00096

[83] P. Ghosal, A. Parui, A. K. Singh, P. Kumbhakar, A. K. Gupta, and C. S. Tiwary, "Porous 3D printed system for synergistic tandem water cleaning-energy generation," *Curr. Sci.*, vol. 125, no. 10, 2023. https://doi.org/10.1002/adsu.202300321

[84] Z. N. Shi, C. Xu, F. Chen, Y. X. Wang, L. Li, Q. T. Meng, and R. Zhang, "Renewable metal-organic-frameworks-coated 3D printing film for removal of malachite green," *RSC Adv.*, vol. 7, no. 79, pp. 49 947–49 952, 2017. https://doi.org/10.1039/C7RA10912A

[85] G. Zhou, K. P. Wang, H. W. Liu, L. Wang, X. F. Xiao, D. D. Dou, and Y. B. Fan, "Three-dimensional polylactic acid@graphene oxide/chitosan sponge bionic filter: Highly efficient adsorption of crystal violet dye," *Int. J. Biol. Macromol.*, vol. 113, pp. 792–803, 2018. https://doi.org/10.1016/j.ijbiomac.2018.02.017

[86] Z. Y. Wang, J. J. Wang, M. Y. Li, K. H. Sun, and C. J. Liu, "Three-dimensional printed acrylonitrile butadiene styrene framework coated with Cu-btc metal-organic frameworks for the removal of methylene blue," *Sci. Rep.*, vol. 4, 2014. https://doi.org/10.1038/srep05939

[87] M. A. Vargas-Muñoz, C. Palomino, G. Turnes, and E. Palacio, "A sampling platform incorporating 3D-printed paddles-stirrers coated with metal-organic framework MIL-100(Fe) for in-situ extraction of phenolic pollutants in biodigester supernatant and wastewater effluent samples," *J. Environ. Chem. Eng.*, vol. 11, no. 5, 2023. https://doi.org/10.1016/j.jece.2023.110503

[88] R. Li, S. Yuan, W. Zhang, H. Zheng, W. Zhu, B. Li, M. Zhou, A. W.-K. Law, and K. Zhou, "3D printing of mixed matrix films based on metal–organic frameworks and thermoplastic polyamide 12 by selective laser sintering for water applications," *ACS Appl. Mater. Interfaces*, vol. 11, no. 43, pp. 40 564–40 574, 2019. https://doi.org/10.1021/acsami.9b11840

[89] Y. H. Miao, W. J. Peng, W. Wang, Y. J. Cao, H. Y. Li, L. P. Chang, Y. K. Huang, G. X. Fan, H. Yi, and Y. L. Zhao, "3D-printed montmorillonite nanosheets based hydrogel with biocompatible polymers as excellent adsorbent for Pb (II) removal," *Sep. Purif. Technol.*, vol. 283, 2022. https://doi.org/10.1016/j.seppur.2021.120176

[90] J. J. Luo, A. P. Ji, G. F. Xia, L. Z. Liu, and J. Yan, "Construction of 3D-printed sodium alginate/chitosan/halloysite nanotube composites as adsorbents of methylene blue," *Molecules*, vol. 29, no. 7, 2024. https://doi.org/10.3390/molecules29071609

[91] K. G. Oliveira, R. Botti, V. Kavun, A. Gafiullina, G. Franchin, E. Repo, and P. Colombo, "Geopolymer beads and 3D printed lattices containing activated carbon and hydrotalcite for anionic dye removal," *Catal. Today*, vol. 390, pp. 57–68, 2022. https://doi.org/10.1016/j.cattod.2021.12.002

[92] X. H. Liu, S. Q. Ma, P. G. He, M. R. Wang, X. M. Duan, D. C. Jia, P. Colombo, and Y. Zhou, "3D printing of green and environment-friendly rGO@ZnO/GP for removal of methylene blue from wastewater," *J. Phys. Chem. Solids*, vol. 174, 2023. https://doi.org/10.1016/j.jpcs.2022.111158

[93] T. Taher, S. A. Muhtar, A. G. N. Sianturi, R. Aflaha, K. Triyana, A. Lesbani, M. F. Arif, D. A. Hapidin, K. Khairurrijal, and Z. L. Yu, "3D-printed Zeolite-MgAl layered double oxides (3D-Ze/LDO) as a reusable adsorbent with dual functionality for effective anionic and cationic pollutant removal from water," *Appl. Clay Sci.*, vol. 278, 2025. https://doi.org/10.1016/j.clay.2025.108009

[94] S. Q. Ma, H. L. Yang, S. Fu, P. G. He, X. M. Duan, Z. H. Yang, D. C. Jia, P. Colombo, and Y. Zhou, "Additive manufacturing of geopolymers with hierarchical porosity for highly efficient removal of Cs," *J. Hazard. Mater.*, vol. 443, 2023. https://doi.org/10.1016/j.jhazmat.2022.130161

[95] S. Q. Ma, H. L. Yang, S. Fu, Y. Hu, P. G. He, Z. L. Sun, X. M. Duan, D. C. Jia, P. Colombo, and Y. Zhou, "Additive manufacturing of hierarchical Zeolite-A lattices with exceptionally high Cs^+ adsorption capacity and near-unity immobilization efficiency," *Chem. Eng. J.*, vol. 474, 2023. https://doi.org/10.1016/j.cej.2023.145909

[96] H. Y. Shen, R. Zou, Y. T. Zhou, X. Guo, Y. N. Guan, D. Na, J. S. Zhang, X. L. Fan, and Y. L. Jiao, "Additive manufacturing of sodalite monolith for continuous heavy metal removal from water sources," *Chin. J. Chem. Eng.*, vol. 42, pp. 82–90, 2022. https://doi.org/10.1016/j.cjche.2021.12.016

[97] W. B. Pathiranage, C. Sharp, C. Williams, A. McKnight, O. Algharibeh, Y. S. Hong, C. Williams, G. Rushing, H. Alkhateb, and M. D'Alessio, "Enhanced ability of 3D-printed bricks to treat wastewater under variable conditions," *J. Environ. Manag.*, vol. 386, 2025. https://doi.org/10.1016/j.jenvman.2025.125690

[98] X. H. Liu, S. J. Zhao, Q. H. Li, P. G. He, X. M. Duan, D. C. Jia, P. Colombo, and Y. Zhou, "Enhancing methylene blue removal performance through interfacial charge transfer effect in 3D printing g-C3N4/geopolymer/Fe (III) composite," *J. Environ. Chem. Eng.*, vol. 13, no. 5, 2025. https://doi.org/10.1016/j.jece.2025.117846

[99] A. Rianjanu, T. Taher, F. Desriani, R. O. Delmita, A. G. N. Sianturi, S. A. Muhtar, B. Ariwahjoedi, N. I. Khamidy, D. R. Adhika, and M. F. Arif, "Examining the influence of sintering temperatures on the efficiency of 3D-printed natural zeolite for methylene blue dye adsorption," *Results Surf. Interfaces*, vol. 17, 2024. https://doi.org/10.1016/j.rsurfi.2024.100337

[100] S. Q. Ma, S. Fu, H. L. Yang, P. G. He, Z. L. Sun, X. M. Duan, D. C. Jia, P. Colombo, and Y. Zhou, "Exploiting bifunctional 3D-printed geopolymers for efficient cesium removal and immobilization: An approach for hazardous waste management," *J. Clean. Prod.*, vol. 437, 2024. https://doi.org/10.1016/j.jclepro.2024.140599

[101] F. Ikhsan, S. A. Muhtar, R. Aflaha, D. R. Adhika, A. Muhyi, K. Triyana, K. Khairurrijal, T. Taher, A. Rianjanu, and M. F. Arif, "Glycerol-assisted modification of 3D-printed zeolite (3D-Ze/Gy) for enhanced methylene blue dye removal in aqueous solutions," *Adv. Eng. Mater.*, vol. 27, no. 9, 2025. https://doi.org/10.1002/adem.202402555

[102] G. Franchin, J. Pesonen, T. Luukkonen, C. Y. Bai, P. Scanferla, R. Botti, S. Carturan, M. Innocentini, and P. Colombo, "Removal of ammonium from wastewater with geopolymer sorbents fabricated via additive manufacturing," *Mater. Des.*, vol. 195, 2020. https://doi.org/10.1016/j.matdes.2020.109006

[103] O. Halevi, T. Y. Chen, P. S. Lee, S. Magdassi, and J. A. Hriljac, "Nuclear wastewater decontamination by 3D-printed hierarchical zeolite monoliths," *RSC Adv.*, vol. 10, no. 10, pp. 5766–5776, 2020. https://doi.org/10.1039/C9RA09967K

[104] N. H. M. Yusoff, C. H. Chong, V. L. Wong, K. H. Cheah, and Y. K. Wan, "The influence of structural topology of additively manufactured PEGDA monolith on adsorption performance for textile wastewater treatment," *Asia-Pac. J. Chem. Eng.*, vol. 18, no. 6, 2023. https://doi.org/10.1002/apj.2952

[105] A. V. O. Akowanou, H. E. J. Deguenon, L. Groendijk, M. P. Aina, B. K. Yao, and P. Drogui, "3D-printed clay-based ceramic water filters for point-of-use water treatment applications," *Prog. Addit. Manuf.*, vol. 4, no. 3, pp. 315–321, 2019. https://doi.org/10.1007/s40964-019-00091-9

[106] A. J. Kennedy, M. L. Ballentine, A. Das, C. S. Griggs, K. Klaus, and M. J. Bortner, "Additive manufacturing for contaminants: Ammonia removal using 3D printed polymer-zeolite composites," *ACS EST Water*, vol. 1, no. 3, pp. 621–629, 2021. https://doi.org/10.1021/acsestwater.0c00131

[107] Y. D. Zhang, B. Zhang, N. S. Li, L. S. Du, Y. Su, K. Du, and W. Zhao, "Additive manufacturing of HA-TCP catalytic porous ceramics by stereolithography technology," *Mater. Chem. Phys.*, vol. 347, 2026. https://doi.org/10.1016/j.matchemphys.2025.131412

[108] A. Figuerola, F. Rodríguez, C. P. Cabello, and G. T. Palomino, "Carbon@ceramic 3D printed devices for bisphenol A and other organic contaminants extraction," *Sep. Purif. Technol.*, vol. 299, 2022. https://doi.org/10.1016/j.seppur.2022.121749

[109] J. Y. Ho, T. T. Chang, P. C. Ho, H. K. Chang, and P. Y. Chen, "Fabrication of gyroid-structured, hierarchically-porous hydroxyapatite scaffolds by a dual-templating method," *Mater. Chem. Phys.*, vol. 314, 2024. https:

//doi.org/10.1016/j.matchemphys.2023.128854

[110] L. C. Li, H. K. Chang, and P. Y. Chen, "Fabrication of hierarchically-porous diatomite scaffolds for dye adsorption by a dual-templating approach," *Ceram. Int.*, vol. 51, no. 16, pp. 22 639–22 652, 2025. https://doi.org/10.1016/j.ceramint.2024.12.005

[111] R. König, M. Spaggiari, O. Santoliquido, P. Principi, G. Bianchi, and A. Ortona, "Micropollutant adsorption from water with engineered porous ceramic architectures produced by additive manufacturing and coated with natural zeolite," *J. Clean. Prod.*, vol. 258, 2020. https://doi.org/10.1016/j.jclepro.2020.120500

[112] M. M. Almeida, N. P. F. Gonçalves, T. Gameiro, Z. Alves, J. A. Labrincha, and R. M. Novais, "3D-printing bauxite residue/fly ash-containing geopolymers as promising metal sorbents for water treatment," *Waste Manag.*, vol. 190, pp. 35–44, 2024. https://doi.org/10.1016/j.wasman.2024.09.007

[113] E. C. Silva, V. R. Soares, A. B. Nornberg, and A. R. Fajardo, "Recyclable 3D-printed composite hydrogel containing rice husk biochar for organic contaminants adsorption in tap water," *ACS Appl. Polym. Mater.*, vol. 5, no. 10, pp. 8415–8429, 2023. https://doi.org/10.1021/acsapm.3c01534

[114] N. P. F. Gonçalves, S. M. Olhero, J. A. Labrincha, and R. M. Novais, "3D-printed red mud/metakaolin-based geopolymers as water pollutant sorbents of methylene blue," *J. Clean. Prod.*, vol. 383, 2023. https://doi.org/10.1016/j.jclepro.2022.135315

[115] N. P. F. Gonçalves, E. F. da Silva, L. A. C. Tarelho, J. A. Labrincha, and R. M. Novais, "Simultaneous removal of multiple metal (loid)s and neutralization of acid mine drainage using 3D-printed bauxite-containing geopolymers," *J. Hazard. Mater.*, vol. 462, 2024. https://doi.org/10.1016/j.jhazmat.2023.132718

[116] M. Asava-arunotai, T. L. Htet, A. Bansiddhi, A. Lertworasirikul, K. Surawathanawises, T. Muangnapoh, B. Kandasamy, P. Kidkhunthod, G. Panomsuwan, and O. Jongprateep, "3D-printed Sr-doped TiO2/biowaste/polymeric structures for mitigating dye contamination in water," *Materialia*, vol. 36, 2024. https://doi.org/10.1016/j.mtla.2024.102139

[117] M. Mahmoud, J. Kraxner, H. Elsayed, D. Galusek, and E. Bernardo, "Advanced dye sorbents from combined stereolithography 3D printing and alkali activation of pharmaceutical glass waste," *Materials*, vol. 15, no. 19, 2022. https://doi.org/10.3390/ma15196823

[118] D. Y. Wang, T. T. Zhi, L. H. Liu, L. Yan, W. Yan, Y. Y. Tang, B. He, L. G. Hu, C. Y. Jing, and G. B. Jiang, "3D printing of TiO2 nanoparticles containing macrostructures for As (III) removal in water," *Sci. Total Environ.*, vol. 815, 2022. https://doi.org/10.1016/j.scitotenv.2021.152754

[119] K. Kim, M. C. Ratri, G. Choe, M. Nam, D. Cho, and K. Shin, "Three-dimensional, printed water-filtration system for economical, on-site arsenic removal," *PLOS ONE*, vol. 15, no. 4, 2020. https://doi.org/10.1371/journal.pone.0231475

[120] J. D. Acuna-Bedoya, J. F. Rangel-Sequeda, M. Loredo-Cancino, M. D. Maya-Trevino, L. P. Dominguez-Jaimes, and J. M. Hernandez-Lopez, "Integration of the adsorption and electro-oxidation process using 3D printed activated carbon monoliths for the degradation of pharmaceutical compounds," *J. Environ. Chem. Eng.*, vol. 10, no. 4, 2022. https://doi.org/10.1016/j.jece.2022.108203

[121] S. Z. Lan, X. S. Xia, Z. Liu, Y. J. Yang, Q. R. Qian, Y. J. Luo, Q. H. Chen, C. L. Cao, and L. R. Xiao, "3D printed cylindrical capsules as a Chlorella pyrenoidosa immobilization device for removal of lead ions contamination," *Front. Chem.*, vol. 10, 2022. https://doi.org/10.3389/fchem.2022.987619

[122] X. Y. Sun, Y. Yan, L. J. Zhang, G. X. Ma, Y. Liu, Y. X. Yu, Q. An, and S. Y. Tao, "Direct 3D printing of reactive agitating impellers for the convenient treatment of various pollutants in water," *Adv. Mater. Interfaces*, vol. 5, no. 8, 2018. https://doi.org/10.1002/admi.201701626

[123] B. Kim, Y. Park, H. W. Kim, J. A. Kim, and Y. Hwang, "Enhanced iodide removal from aqueous solutions using 3D-printed PLA scaffold coated with Cu/Cu2O nanoparticles," *Environ. Res.*, vol. 279, 2025. https://doi.org/10.1016/j.envres.2025.121835

[124] X. Xia, X. Xu, C. Lin, Y. Yang, L. Zeng, Y. Zheng, X. Wu, W. Li, L. Xiao, Q. Qian *et al.*, "Microalgal-immobilized biocomposite scaffold fabricated by fused deposition modeling 3D printing technology for dyes removal," *ES Mater. Manuf.*, vol. 7, pp. 40–50, 2020. https://doi.org/10.30919/esmm5f706

[125] Y. C. Ji, Y. Ma, Y. J. Ma, J. Asenbauer, S. Passerini, and C. Streb, "Water decontamination by polyoxometalate-functionalized 3D-printed hierarchical porous devices," *Chem. Commun.*, vol. 54, no. 24, pp. 3018–3021, 2018. https://doi.org/10.1039/C8CC00821C

[126] C. Z. Yan, H. W. Fan, D. R. Huang, and G. Wang, "A 2D mixed fracture-pore seepage model and hydromechanical coupling for fractured porous media," *Acta Geotech.*, vol. 16, no. 10, pp. 3061–3086, 2021. https://doi.org/10.1007/s11440-021-01183-z

[127] W. H. Lei, X. K. Lu, W. B. Gong, and M. R. Wang, "Triggering interfacial instabilities during forced imbibition by adjusting the aspect ratio in depth-variable microfluidic porous media," *Proc. Natl. Acad. Sci. U.S.A.*, vol. 120, no. 50, 2023. https://doi.org/10.1073/pnas.2310584120

[128] A. Subash, V. Gajare, M. Naebe, and B. Kandasubramanian, "Experimental and machine learning investigation of poly-ϵ-caprolactone-MXene composites for methylene blue capture," *ChemistrySelect*, vol. 10, no. 37, 2025. https://doi.org/10.1002/slct.202503397

[129] F. Mashkoor, S. M. Adnan, M. Shoeb, and C. Jeong, "Waste-to-wealth strategy: Ti3AlC2-max-supported WS2/Halloysite nanocomposite for the removal of nickel metal ions from wastewater with machine learning simulation and subsequent application in supercapacitors," *ACS Sustainable Chem. Eng.*, vol. 12, no. 17, pp. 6547–6563, 2024. https://doi.org/10.1021/acssuschemeng.3c08132

[130] M. Claverie, J. Garcia, T. Prevost, J. Brendlé, and L. Limousy, "Inorganic and hybrid (organic-inorganic) lamellar materials for heavy metals and radionuclides capture in energy wastes management: A review," *Materials*, vol. 12, no. 9, 2019. https://doi.org/10.3390/ma12091399

[131] W. F. Hao, J. N. Zhang, and W. F. Yan, "Application of zeolite in the radioactive wastewater treatment," *Chin. Sci. Bull.*, vol. 69, no. 16, pp. 2221–2232, 2024. https://doi.org/10.1360/TB-2023-0799

[132] C. Schweiker, S. Zankovic, A. Baghnavi, D. Velten, H. Schmal, R. Thomann, and M. Seidenstuecker, "Core-shell 3D printed biodegradable calcium phosphate cement-alginate scaffolds for possible bone regeneration applications," *Front. Drug Deliv.*, vol. 4, 2024. https://doi.org/10.3389/fddev.2024.1452132

[133] T. R. Chen, K. Renn, A. Das, D. Kazerooni, J. E. Han, D. A. Okonski, Y. M. Yao, C. Q. Pritchard, L. Ju, C. D. Mansfield *et al.*, "Highly stiff and strong fiber reinforced core-shell composites for 3D printing," *Polym. Compos.*, vol. 46, no. 8, pp. 6858–6872, 2025. https://doi.org/10.1002/pc.29396

[134] F. D. Hong, B. Lampret, C. Myant, S. Hodges, and D. Boyle, "5-axis multi-material 3D printing of curved electrical traces," *Addit. Manuf.*, vol. 70, 2023. https://doi.org/10.1016/j.addma.2023.103546

[135] M. O. F. Emon, F. Alkadi, D. G. Philip, D. H. Kim, K. C. Lee, and J. W. Choi, "Multi-material 3D printing of a soft pressure sensor," *Addit. Manuf.*, vol. 28, pp. 629–638, 2019. https://doi.org/10.1016/j.addma.2019.06.001

[136] Y. H. Li, H. Li, Y. R. Zhou, Q. Xia, M. Yi, J. W. Shang, and X. W. Cheng, "Efficient adsorption performance and mechanism of fluoroquinolone antibiotic onto the acid wash-assisted Co NPs/N-c adsorbent," *Sep. Purif. Technol.*, vol. 353, 2025. https://doi.org/10.1016/j.seppur.2024.128457

[137] L. H. Liu, T. Li, J. Y. Liu, B. Q. Hu, Z. H. Zhou, and A. P. Tang, "Synthesis of mesoporous calcium silicate by template method and its adsorption characteristic for Pb^{2+}," in *the 3rd International Conference on Green Materials and Environmental Engineering (GMEE)*, Beijing, China, 2017, pp. 212–219.

[138] G. Lee, I. Ahmed, H. J. Lee, and S. H. Jhung, "Adsorptive removal of organic pollutants with a specific functional group from water by using metal-organic frameworks (MOFs) or MOF-derived carbons: A review," *Sep. Purif. Technol.*, vol. 347, 2024. https://doi.org/10.1016/j.seppur.2024.127602